Miner Petrol (2009) 96:19–41
DOI 10.1007/s00710-009-0042-9

ORIGINAL PAPER

U–Pb dating, Hf-isotope characteristics and trace-REE-patterns of zircons from Medet porphyry copper deposit, Bulgaria: implications for timing, duration and sources of ore-bearing magmatism

Irena Peytcheva · Albrecht von Quadt · Franz Neubauer · Martin Frank · Rossen Nedialkov · Christoph Heinrich · Strashimir Strashimirov

Received: 18 January 2008 / Accepted: 2 January 2009 / Published online: 24 January 2009

Abstract Precise U–Pb geochronology, Hf isotope compositions and trace element distributions in zircons are combined in the present study to define the timing and sources of the magmatism forming the Medet porphyry copper deposit, Bulgaria. ID-TIMS U–Pb-zircon dating demonstrates that ore-bearing magmatism extended for less than 1.12 Ma. As inferred from the field relationships, it started with the intrusion of a quartz-monzodiorite at 90.59±0.29 Ma followed by granodiorite porphyries at 90.47±0.30 and 90.27±0.60 Ma and by crosscutting aplite dykes at 90.12±0.36 Ma. These units were overprinted by potassic alteration and host economic copper-(Mo–Au) mineralization. The main magmatic–hydrothermal activity ceased after that, and a later quartz-granodiorite porphyry dyke, dated at 89.26±0.32 Ma, only contains an uneconomic quartz–pyrite mineralization. Assimilation of Lower Paleozoic rocks with a mantle to mantle–crust signature is characteristic of the fertile magma in the Medet deposit, as defined by positive ε-Hf values of the inherited zircons. The positive Ce-anomalies and the higher Eu/Eu* ratios of the zircons in the mineralized Cretaceous rocks of Medet deposit argue for crystallization from a generally more oxidized magma compared to the later quartz-granodiorite porphyry dyke. A change in paleostress conditions occurred during the intrusion of the Medet pluton and its dykes. The initial stage reveals E–W extension associated with N–S compression, whereas the younger granodiorite dyke was emplaced during subsequent N–S extension. The large-scale switch of the extensional stress regime during the mineralization was favourable for ore deposition by channelling the fluids and increasing the effective permeability.

Editorial handling: A. Möller

Electronic supplementary material The online version of this article (doi:10.1007/s00710-009-0042-9) contains supplementary material, which is available to authorized users.

I. Peytcheva · A. von Quadt (✉) · M. Frank · C. Heinrich
Institute of Isotope Geochemistry and Mineral Resources,
ETH Zurich,
Zurich, Switzerland
e-mail: quadt@erdw.ethz.ch

I. Peytcheva
Geological Institute, Bulgarian Academy of Science,
Sofia, Bulgaria

F. Neubauer
Institute of Geology and Palaeontology, University of Salzburg,
Salzburg, Austria

R. Nedialkov
Faculty of Geology and Geography,
Sofia University "St. Kliment Ochridski",
Sofia, Bulgaria

S. Strashimirov
University of Mining and Geology "St. Ivan Rilski",
Sofia, Bulgaria

Present address:
M. Frank
IFM-GEOMAR,
Leibniz Institute for Marine Sciences at the University of Kiel,
Kiel, Germany

Introduction

The Medet deposit is situated in the central area of the Srednogorie tectonic zone in Bulgaria (Fig. 1a, b). It is part of the Apuseni–Banat–Timok–Srednogorie belt (Popov et

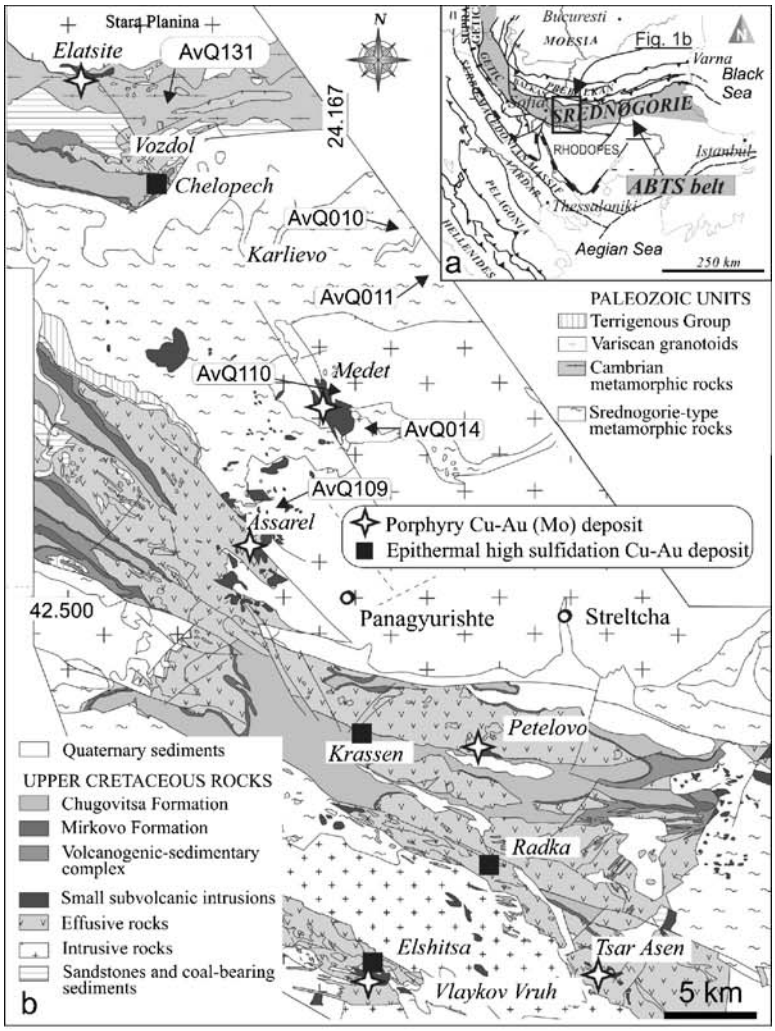

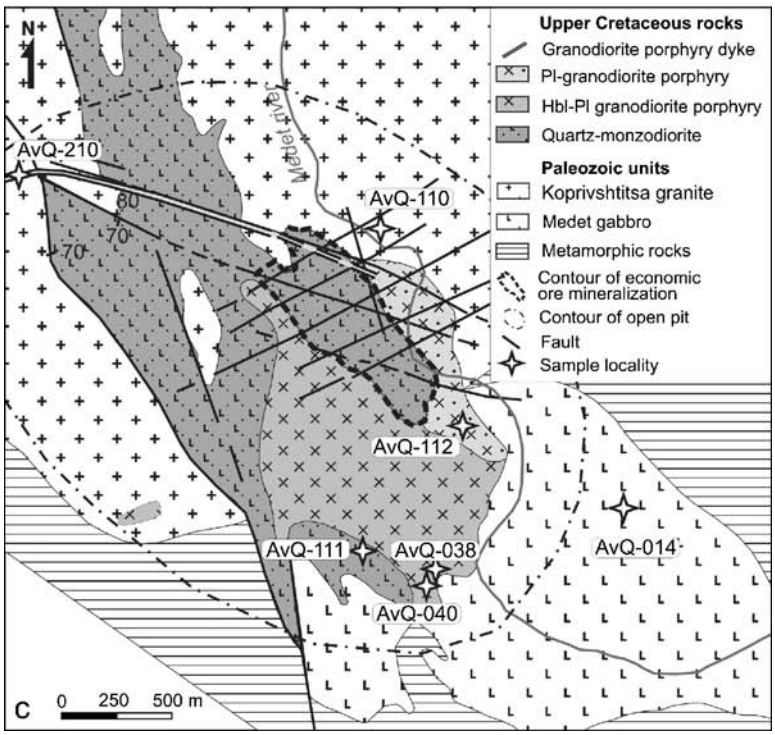

Fig. 1 *a* Tectonic sketch map of the Balkan peninsula (after Sandulescu 1984) with the position of the Apuseni–Banat–Timok–Srednogorie (ABTS) belt; *b* geological map of the Panagyurishte region of Central Srednogorie (after Strashimirov and Popov 2000, modified by Chambefort and Moritz 2006) with the location of the main porphyry copper and Cu–Au epithermal deposits; the arrows show the position of the samples from the basement, which were used for geochemical interpretations (see text); *c* simplified geological map of the area of the Medet deposit (modified after Ushev et al. 1962 and Popov and Bayraktarov 1978) with sample localities

al. 2000a, b; von Quadt et al. 2005) of broadly calc-alkaline Upper Cretaceous magmatism which hosts Europe's major porphyry Cu–Mo–Au deposits (Janković 1977; Vassileff and Stanisheva-Vassileva 1981; Popov et al. 1996; Berza et al. 1998; Ciobanu et al. 2002; Heinrich and Neubauer 2002; Kamenov et al. 2007). As it was the first copper-porphyry type deposit mined in Eastern Europe (discovered in 1955; Ushev et al. 1962) Medet became important for the progress of the mining industry of the whole region. 163 million tons (Mt) of ore have been mined from Medet deposit in the period 1964–1993 at an average grade of 0.32% Cu and 0.1 g/t Au (Strashimirov et al. 2002). There is still about 48 Mt of 0.29 Cu% ore (Milev et al. 1996) left in the deposit as mining became uneconomical at greater depth.

The formation of the Medet deposit is related to a shallow Upper Cretaceous intrusion—the Medet pluton (Ushev et al. 1962; Popov et al. 1996). It consists of consecutively intruded dykes and subvolcanic bodies of intermediate composition. In the present study we describe them with respect to the overprinting hydrothermal alteration and hosting of the economic porphyry-copper mineralization, with the aim to bracket the timing of ore-related magmatism. For constraining the age of the magmatic pulses we used the U–Pb ID-TIMS (isotope dilution-thermal ionization mass-spectrometry) method, which is the most precise method for dating igneous rocks (usually 0.3–0.1% 2 sigma errors, using a ^{205}Pb–^{235}U isotope tracer, e.g. see summary in Parrish and Noble 2003; von Quadt et al. 2005). The high precision is particularly important, because in several large porphyry-hosting magmatic–hydrothermal systems the emplacement, mineralization, and cooling associated with individual porphyry stocks are estimated as spanning only about 10,000 to 200,000 years (e.g., Marsh et al. 1997; Halter et al. 2004; Harris et al. 2004). On the deposit scale, multiple intrusions of magma may provide additional energy (temperature), leading to heating and convection of the hydrothermal fluids. Yet the fertile magmatism related to ore-formation usually lasted less than 1 Ma (von Quadt et al. 2002, 2005; Stoykov et al. 2004; Halter et al. 2004; Kouzmanov et al. 2006; Zimmerman et al. 2008). For the Medet deposit, however, the published K–Ar and Ar–Ar isotope data (Lilov and Chipchakova 1999; Handler et al. 2004; Lips et al. 2004) provide evidence for a long-lived magmatic–hydrothermal system of more than 10 Ma. This data can be tested using the U–Pb zircon method, as the refractory zircon is generally not susceptible to age resetting during low-temperature hydrothermal overprinting, and the effects of radiogenic lead loss can be avoided through mechanical or chemical abrasion of the studied grains.

The present study aims to contribute to the understanding of the specific characteristics of the magma that was responsible for the formation of the deposit (in the following we will use the term "fertile" for this magma). In Medet it was enriched not only in Cu and in Mo, but contained also base metals, precious and platinum-group elements (PGE; Tarkian and Stribrny 1999; Strashimirov et al. 2002). For this purpose, we combined the whole-rock geochemistry with the hafnium (Hf) isotope characteristics and the trace and rare earth element (REE) distributions of the zircons. To avoid incorrect interpretation (e.g. zircon inheritance) the conventional single zircon data are complemented with in-situ Laser Ablation Inductively Coupled Plasma Mass Spectrometry (LA-ICP-MS) zircon dating and in-situ Multiple-Collector (MC)-LA-ICP-MS hafnium isotope measurements. The uncertainties of the in-situ LA-ICP-MS dating are considerable larger (average of 2–5% 2 sigma uncertainties) than the ID-TIMS analyses, therefore, the in-situ ages are used only for age-corrections and interpretations of the Hf isotope data and the trace element data of the zircons. The isotope and geochemical data are combined with the structural data from the region of the deposit to better constrain the geodynamic evolution and time relationships of the magmatic and hydrothermal products and to infer possible changes during the ore-forming processes in Medet.

Geological background and sampling

Regional position

The Srednogorie zone in Bulgaria is considered part of the internal sectors of the Alpine–Balkan–Carpathian–Dinaride orogen, which consist of pre-Alpine basement and were affected by Cretaceous tectonic events (e.g. Neubauer et al. 2003). The Upper Cretaceous magmatic activity is related to a northward subduction and to a back-arc/intra-arc tectonic setting (e.g. Boccalett et al. 1978; von Quadt et al. 2005; Schmid et al. 2008; Georgiev 2008). Seismic tomography studies have illustrated the long history (~100 million years) of the subduction of the lithosphere at the southern margin of Europe (Wortel and Spakman 2000), with the Srednogorie zone representing the oldest stage of magmatism in this evolution, starting at ca. 92 Ma on the southern passive margin of Europe (Moesian Platform; e.g. Lips 2002; Neubauer 2002). The general younging of the magmatism in Central Srednogorie from ~92 Ma in the north to ~78 Ma in the south is explained as a consequence of slab retreat during oblique subduction (Neubauer 2002; Lips 2002; Handler et al. 2004; von Quadt et al. 2005; Kamenov et al. 2007).

Geological setting of the Medet deposit

The Medet deposit is situated in the central parts of the Central Srednogorie zone—also called the Panagyurishte

district (Fig. 1b). The pre-Alpine basement of the deposit is represented by high-metamorphic rocks of mainly continental origin and consists of two-mica gneisses and gneissose schists, mica schists, orthoamphibolites, small serpentinite bodies and anatexites (Dimitrova and Belmustakova 1982). The region of the Medet deposit (Fig. 1c) consists of gneisses and rare amphibolites with Lower Paleozoic and older protoliths (Carrigan et al. 2006; Peytcheva and von Quadt 2004), which were metamorphosed at 336.5±5.4 Ma (Carrigan et al. 2006). Late Carboniferous granites, granodiorites and gabbros (Dabovski et al. 1972; Bojadjiev 1993; Peytcheva and von Quadt 2004; Carrigan et al. 2005) with collisional (Koprivshtitsa pluton) and post-collisional characteristics (Smilovene pluton and Medet gabbro) intruded the metamorphic rocks.

This Variscan basement is intruded by the Medet pluton (Ushev et al. 1962)—a small shallow stock-like body with an exposure area of ~3 km^2 (Fig. 1c), which according to geophysical data represents the apophysis of a deeper seated larger intrusive body (Tsvetkov et al. 1978). The Medet shallow pluton is composed of the following main phases (Chipchakova 2002; Strashimirov et al. 2002; Figs. 1c and 2): (i) quartz-monzodiorites (equigranular and rarely porphyritic); (ii) granodiorites, as well as transitional to quartz-diorite (porphyritic); and (iii) aplite veins. Angelkov (1984) also described explosive breccias of quartz-monzodiorite composition. One "late dyke" (with probable lamprophyric composition according to Todor Marinov, personal communication) cross cuts the two main rock types and the granites of Koprivshtitsa pluton. The whole succession of shallow plutonic and subvolcanic bodies, dykes and volcanic breccias let exploration geologists to infer that an eroded volcanic edifice was located on top of the now exposed Medet region (Angelkov 1984; Bogdanov 1987). Alternative interpretations consider the Assarel volcanic and subvolcanic rocks (Fig. 1b) as the missing volcanic succession (Strashimirov and Popov 2000; Chipchakova 2002).

Structural geology

Three main fault systems are described in the deposit (Angelkov 1982, 1984): NW (~N115–125 trending), NE (~N50 trending) and ~E–W trending (~N80–100). Popov and Bayraktarov (1978), Popov et al. (1996) and Popov and Popov (2000) pointed out the complicated morphology of the intrusion, which is elongated in a south–southeastern direction (150°), about parallel to the regional trend of ore deposits in the Panagyurishte ore district. The ore-deposition was related to the NW (~N115–120 trending) and NE (~N50 trending) faults, steeply dipping to SW and SE, respectively. The Upper Cretaceous rocks of the Medet deposit together with their hosting Variscan basement rocks are uplifted towards the Assarel volcanic and subvolcanic rocks along

Fig. 2 Field relationships and sampled rocks of the Medet deposit: **a** Q-monzodiorite (Q-Mzdr) (AvQ111), crosscut by Pl-Hbl-porphyry granodiorite vein; **b** enclave of Q-monzodiorite in the granodiorite porphyry with phenocrysts of Pl and Hbl (Pl-Hbl-granodiorite porphyry), both crosscut by aplite veins; **c** contact of the granodiorites with phenocrysts of Pl (AvQ112) and Hbl and Pl (AvQ038); **d** steep-dipping aplite veins (AvQ040) crosscutting the Pl-Hbl-granodiorite porphyry; **e** late granodiorite dyke (AvQ210). *Q* quartz, *Pl* plagioclase, *Hbl* hornblende

the Mialski fault striking NNW (310°) (Angelkov 1984; Ignatovski 1979).

Additionally, we measured the orientation of aplitic dykes, veins and fractures of the Medet deposit. Within the Medet pluton, aplitic dykes strike predominantly N–S (Fig. 3a). In contrast, the Q-granodiorite dyke (AvQ210) trends WNW–ESE (Fig. 1c), nearly perpendicular to the aplite dykes and quartz veins. Quartz veins display two sets: (1) subvertical quartz-filled veins trending N–S, and (2) veins of another set trending NE–SW and dipping variably to SE (Fig. 3b). We also measured a number of brittle fault planes which postdate all dykes and veins. They occur in two sets which are consistent with the orientation of the map-scale faults. One set trends WNW and displays a dextral displacement; the second, sinistral set trends NNW to N (Fig. 3c). Both sets are characterized by subhorizontal striations underlining their origin as strike-slip faults. Using standard paleostress assessment programs (Ortner et al. 2002), a NW–SE maximum principal orientation direction can be deduced (Fig. 3c, P-axis in the NW sector; P = pressure).

Consequently, our structural data give evidence for a two different paleostress orientations. Aplite dykes originated by E–W extension, as did the quartz veins. The late granodiorite dyke is a result of NNE–SSW extension indicating a late overprinting with NW–SE compression.

Alteration and mineralization

Porphyry style ore formation in the Medet deposit occurs as a result of progressive solidification, fracturing, magmatic fluids exsolution and deposition of the ores in fractures (mainly in the quartz-monzodiorites) or by replacement of mafic minerals or accessory magnetite (Ushev et al. 1962; Chipchakova 2002; Strashimirov et al. 2002). Ushev et al. (1962) established two main types of ore-related hydrothermal wall-rock alteration in the Medet deposit: potassic (K)-silicate alteration (metasomatic K-feldspar and biotite, quartz and apatite) and propylitic alteration (chlorite, epidote and carbonate). Popov et al. (2000a, b) inferred a pre-ore K-silicate alteration, a syn-ore propylitic type alteration (epidote, chlorite, sericite) and a post-ore carbonate–zeolite association. Recently Chipchakova (2002) distinguished three alteration types in the deposit, which are typical of porphyry-copper deposits: (1) an outer, propylitic zone with a mineral association (paragenesis) of epidote, chlorite, actinolite ± pyrite; (2) a middle, sericite zone with a paragenesis of quartz, sericite and pyrite (i.e. phyllic alteration); and (3) an inner, K-silicate zone (i.e. potassic alteration) with K-feldspar, biotite, quartz, apatite, magnetite, pyrite, chalcopyrite ± molybdenite ± bornite. Chipchakova (2002) described two types of hydrothermal biotite: a metasomatic and a vein type biotite. Both are not altered at the contact to the sulfide minerals, which is evidence that the potassic alteration formed in equilibrium with the main ore mineralization.

Strashimirov et al. (2002) distinguished six mineral associations in the deposit. The earliest (i) quartz–magnetite–hematite ore-mineral association is related to the K-silicate alteration. It is overprinted by (ii) the propylitic alteration, containing Ti-bearing minerals (rutile, ilmenite, Mn-ilmenite, pseudobrookite and davidite). The pervasive main economic assemblage (iii) quartz–pyrite–chalcopyrite is disseminated in the host rocks, or occurs in short veins and veinlets. It is accompanied by molybdenite and by a specific Co–Ni assemblage and rare Cu–Sn–V and Bi–Ag–Te assemblages (Strashimirov et al. 2002). Molybdenite also occurs in veinlets of the next (iv) quartz–molybdenite association. The (v) quartz–pyrite association forms well-defined veins and veinlets in the central part of the deposit, while the (vi) quartz–galena–sphalerite association is occasionally observed as small veins in the upper and marginal parts of the deposit. Secondary copper minerals are rarely found along faults and mainly occur in the upper parts of the Medet deposit (Ushev et al. 1962; Strashimirov et al. 2002).

Chipchakova (2002) considered the Cu–(Mo) mineralization in the Medet deposit as having formed in two main phases: a first main stock-work type mineralization was followed by subordinate vein-type mineralization. The latter occurs in the SE parts of the deposit, mainly along NE faults. These veins are 2–3 cm, rarely up to 10 cm wide and cut the main copper-porphyry ore body as well as the granodiorite porphyries. They consist of quartz, pyrite,

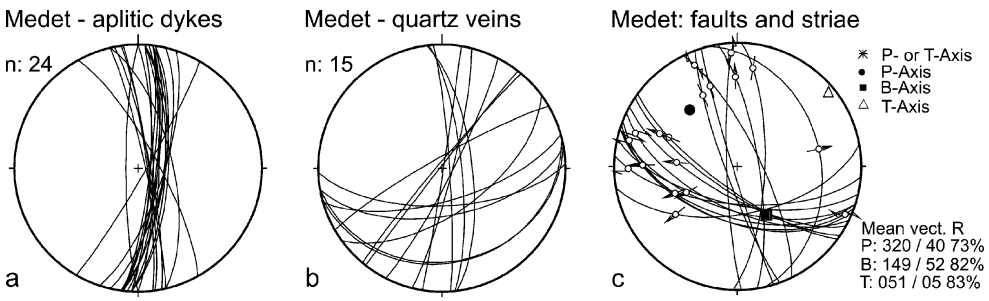

Fig. 3 Orientations of **a** aplite dykes (N–S-trending), **b** quartz veins (N–S and NE–SW trending) and **c** faults in the Medet deposit. The faults post-date mineralization and correspond to the orientations of regional scale faults (Fig. 1c)

chalcopyrite ± molybdenite ± hematite and are associated with propylitic type alteration (epidote, chlorite, quartz, albite and sericite; Chipchakova 2002).

Based on homogenization temperatures of fluid inclusions in potassium feldspar from the K-silicate alteration zone the temperature of the primary magmatic fluids was estimated to be 610–680°C (Chipchakova 2002). With decreasing temperature, the fluids became more and more diluted by meteoric water (Strashimirov 1982; Strashimirov and Kovachev 1992; Strashimirov et al. 2002) and at the end of hydrothermal mineral precipitation, when the calcite–zeolite association filled fractures and fine fissures in the host rocks (Popov et al. 2000a, b) or in the ore-veins (Chipchakova 2002), the salinity of the fluids was very low.

Previous age data

Published geochronological data suggest a magmatic and a hydrothermal activity over more than 10 Ma and are usually considered as corresponding to multiple intrusions of subvolcanic bodies and dykes (e.g. Chipchakova and Lilov 1976; Bogdanov 1987; Popov et al. 2000a, b) and/or two episodes of magmatic–hydrothermal activity and ore mineralization (Chipchakova 2002; Lips et al. 2004). Published K–Ar ages range from 90–88 Ma for the ore-related and ore-hosting Q-monzodiorite to 75–78 Ma for the subvolcanic granodiorite porphyries (Chipchakova and Lilov 1976). The K-silicate alteration was dated at 88–87 Ma, and sericite at ~79 Ma by the same authors (Lilov and Chipchkova 1999). The $^{40}Ar/^{39}Ar$ dating of "igneous biotite" from the quartz-monzodiorite yields a cooling age of 90.4±0.9 (Lips et al. 2004), whereas the age of hornblende from a granodiorite sample was determined at 85.7 Ma (Handler et al. 2004). White micas (sericite) from Medet yielded plateau ages of 79.0±0.8 to 79.5±0.7 Ma and are consistent with the K–Ar ages. Recently, Zimmerman et al. (2008) reported Re–Os molybdenite ages between 90.55 and 91.3 Ma suggesting a short-lived magmatic–hydrothermal system.

Sampling

For the present study, we dated the main rock types in the Medet deposit (Fig. 1c) considering the relative time succession inferred from field observations (Fig. 2) and from the published data. Sample AvQ111 is a quartz-monzodiorite (Fig. 2a), AvQ112 and AvQ038 are granodiorite porphyries with plagioclase (Pl) and hornblende–plagioclase (Hbl-Pl) phenocrysts, respectively (Fig. 2c, b; for convenience they will be called Pl- and Hbl-Pl granodiorite porphyries further in the text). The latter are cross-cut by aplitic veins (AvQ040, Fig. 2b, d). All these rocks were overprinted by K-silicate alteration and host economic copper–(Mo–Au) mineralization. Finally the "late dyke" was sampled (AvQ210, Fig. 2e), which is defined as granodiorite porphyry with phenocrysts of quartz (Q) (or Q-granodiorite porphyry for brevity). This dyke is from the propylitic zone of the deposit and contains only minerals of a non-economic quartz–pyrite assemblage. All the samples are from the middle and upper parts of the Medet open pit because the deposit is now closed for production and its central parts have either been exploited or are inaccessible. Consequently, most observations about the relationship of the timing of magmatism to economic hydrothermal ore mineralization are based on published data (summarized above) combined with our own observations in the outer parts of the Medet deposit.

The samples of the Upper Cretaceous rocks are complemented with samples of the basement rocks (Fig. 1b, c). AvQ131 is a metadiabase from the low-grade metamorphic Berkovitsa Group in the adjacent Stara Planina area; AvQ110 is from the Variscan Koprivshtitsa Granite and AvQ014 from the Variscan gabbro in the region of the Medet deposit; AvQ109 is sampled from the Smilovene Granite of the Assarel deposit; AvQ010 is a high-grade metamorphic gneiss, and AvQ011 an amphibolite, both cropping out NE of the deposit.

Analytical techniques

Major and trace elements in rocks

Major element analyses on whole rocks were carried out on Li-tetraborate pellets using the X-ray fluorescence (XRF) method at ETH-Zurich (data presented in Table 1). Trace element and REE determinations were conducted with Laser Ablation Inductively Coupled Plasma-Mass Spectrometry (LA-ICPMS) on the same Li-tetraborate pellets. LA-ICPMS spot analyses were done using an Excimer laser (ArF 193 nm) with a gas mixture containing 5% fluorine in Ar with small amounts of He and Ne, connected to a PE SCIEX Elan 6000 ICP-MS instrument at ETH Zurich. For the present study a spot diameter of 40 μm was used. The reproducibility of analyses was estimated by repeated measurements of the NIST 610 standard. For further details the reader is referred to Günther et al. (2001) and Halter et al. (2004).

Laser ablation ICPMS (LA-ICP-MS) analyses of zircon

Laser ablation ICP-MS spot analyses were done using the same Excimer laser (ArF 193 nm) and PE SCIEX Elan 6000 ICP-MS at ETH, Zurich as for the trace element analyses of the whole rock samples. The zircon pellet (after CL imaging) was placed in a closed cell together with the

Table 1 Major and trace element composition of dated samples from Medet deposit

	AvQ111	AvQ112	AvQ038	AvQ040	AvQ210	AvQ010	AvQ011	AvQ014	AvQ109	AvQ110	AvQ131
	Upper Cretaceous magmatic rocks					Basement rocks					
	Q-Monzdr porphyry	Pl-Gdr porphyry	Hbl-Pl-Gdr porphyry	Aplitic vein	Q-Gdr porphyry	Gneiss	Amphi-bolite	Var Medet gb	Var Smilo-vene gr	Var Koriv-shitsa gr	Pz Meta-diabase
SiO_2	59.20	63.28	64.48	74.87	65.40	63.71	45.22	55.5	65.99	71.17	52.23
TiO_2	0.60	0.42	0.52	0.16	0.48	0.80	1.22	0.58	0.40	0.11	1.33
Al_2O_3	18.36	17.92	14.50	12.41	15.24	16.25	16.04	14.56	15.36	16.93	13.67
FeO	3.98	4.30	4.30	1.60	4.10	6.32	12.46	8.4	3.76	0.94	9.44
MnO	0.09	0.10	0.14	0.02	0.10	0.10	0.29	0.14	0.10	0.02	0.24
MgO	2.64	1.78	1.92	0.28	1.89	2.70	6.94	10.16	2.19	0.39	5.75
CaO	5.70	5.11	5.51	0.93	1.86	1.81	11.22	8.14	3.64	1.05	7.83
Na_2O	3.54	4.06	3.96	2.47	4.07	2.93	2.26	2.39	3.49	3.61	2.94
K_2O	3.14	3.55	3.08	5.77	3.93	3.01	1.26	0.74	2.72	5.03	0.02
P_2O_5	0.20	0.23	0.39	0.02	0.14	0.17	0.66	0.08	0.08	0.21	0.14
LOI	0.86		0.77	0.72	2.71	2.04	2.22	0.68	1.78		7.09
Total	98.13	100.74	99.57	99.25	99.91	99.87	99.81	101.37	99.51	99.48	100.69
Sc	13.9	7.95		1.83	9.29	17.2	32.5	28.5	9.70	3.85	30.03
Cr	248	349	20	361	115	103	37.7	704	240	468	226
Co	14.05	9.42	9.0	2.13	10.4	17.2	36.7	36.9	8.74	1.72	33.0
Ni	14.64	28.4	4.0	15.0	23.8	44.8	20.3	217	28.4	19.0	94.5
Cu	552	60.4	51	30.50	171	26.4	161	51.5	11.1	222	71.8
Zn	28.7	37.2	44	19.07	50.1	85.9	128	59.0	49.8	14.0	98.4
Ga	17.8	20.2	17	11.47	32.34	20.1	16.9		14.6	15.7	19.7
As	154	197	4.0	2.08	5.53	1.87	2.24	1.36	65.3	66.9	480
Rb	83.8	95.0	115	174	109.0	129	46.7	23.2	72.4	126	0.69
Sr	873	861	852	167	396.9	253	351	248	302	304	365
Y	18.7	16.2	19.0	6.16	14.6	30.1	24.8	20.2	13.1	14.9	38.1
Zr	117	115	87.0	75.1	96.9	217	67.1	95.9	101	56.6	288
Nb	5.15	6.13	5.0	4.47	5.62	11.9	5.31	3.53	6.10	6.19	14.0
Mo	8.87	9.19		5.18	1.79	0.77	1.11	0.70	2.87	214	3.86
Cs	1.45	1.23	15.0	1.38	4.81	5.28	1.04	1.14	0.95	1.65	0.15
Ba	505	630	542	259	629	571	284	249	563	852	72.3
La	28.0	31.1	44.0	24.3	26.8	35.9	22.4	12.7	24.1	13.9	22.9
Ce	56.4	55.4	52.0	26.0	47.9	68.4	51.9	28.1	43.3	26.6	47.9
Pr	6.56	6.12		2.96	5.47	8.16	6.87	3.75	4.31	3.12	6.07
Nd	28.3	23.5	27.0	28.4	18.9	33.1	31.6	15.9	16.5	12.4	27.6
Sm	5.91	4.83		1.13	3.38	6.92	6.42	3.89	2.92	2.76	6.66
Eu	1.57	1.24		0.21	1.12	1.51	1.89	0.88	0.77	0.62	1.82
Gd	4.49	2.91		0.69	2.41	6.39	6.00	3.38	2.27	2.61	6.62
Tb	0.63	0.46		0.14	0.41	0.84	0.75	0.58	0.39	0.46	1.24
Dy	3.56	2.90		0.91	2.17	5.23	4.57	3.43	2.32	2.82	7.15
Ho	0.66	0.60		0.16	0.56	1.14	0.84	0.74	0.52	0.51	1.52
Er	1.84	1.52		0.77	1.52	3.14	2.78	2.03	1.44	1.20	4.11
Tm	0.28	0.28		0.13	0.20	0.41	0.35	0.31	0.27	0.17	0.63
Yb	1.97	1.89		1.04	1.30	3.45	2.35	1.98	1.55	1.06	4.69
Lu	0.30	0.30		0.12	0.23	0.46	0.36	0.30	0.18	0.19	0.63
Hf	3.10	2.64	6.0	2.91	2.95	5.68	1.60	2.49	3.05	1.99	6.99
Ta	0.27	0.44		0.45	0.49	0.73	0.29	0.21	0.62	0.72	0.74
Pb	11.6	87.8	8.0	26.1	14.7	14.4	6.47	6.54	19.8	34.0	105
Th	6.94	9.78	7.0	21.6	8.93	12.7	5.02	2.01	15.2	4.42	2.99
U	1.92	3.03	2.0	3.02	2.31	2.58	1.17	0.69	5.62	3.68	0.79
W	6.09			2.98	1.52	1.09	0.28	0.54	5.27	15.4	
V	203		126	25.3	116	108	295		82.2	40.7	

Major oxides in wt.%, trace and rare earth elements (REE) in ppm
Q quartz, *monzdr* monzodiorite, *Pl* plagioclase, *Hbl* hornblende, *Gdr* granodiorite, *gr* granite, *gb* gabbro, *Var* Variscan, *Pz* Palaeozoic

standard material (NIST 610) from which the ablated material is carried to the ICP-MS by an argon gas stream. We used spot diameters of 40 and 20 μm with a laser pulse repetition rate of 10 Hz. Elemental abundances were detected with 10 ms dwell time and 3 ms quadrupole settling time. The measurement efficiency was around 70%. Backgrounds were measured for 30 s and the transient signals from the sample material were acquired for about 30 s. Calibrations for the zircon analyses were carried out using NIST 610 glass as an external standard. Limits of detection are calculated as three times the standard deviation of the background normalized to the volume of the sample ablated (cps/μg/g). The reproducibility of the data during this work was estimated measuring the NIST 610 standard.

The in-situ LA-Quadrupole-ICPMS age measurements (U–Th–Pb method) were carried out at ETH Zurich using time resolved analyses (TRA) operated in fast peak-hopping and DUAL detector mode using a short integration time. Again, zircon mounts (after CL imaging) were placed in a closed cell together with the external standard material. The protocol for U–Pb of the zircons was performed at laser frequency of 10 Hz and a spot size of 40 μm. It starts with a 30 s baseline measurement and then the raw count rates of ^{29}Si, ^{202}Hg, ^{204}Pb, ^{206}Pb, ^{207}Pb, ^{208}Pb, ^{232}Th, and ^{238}U were measured using Q-ICPMS. A mercury correction using ^{202}Hg/^{204}Hg ratio was not applied, because of the low ^{204}Pb and ^{202}Hg intensities. For external calibration we used both, the NIST SRM 610 standard and Plešovice standard zircon. Concentration values of NIST SRM 610 were taken from Pearce et al. (1997) and for the Plešovice zircon from Slama et al. (2008). The ^{207}Pb/^{206}Pb, ^{206}Pb/^{238}U, ^{207}Pb/^{235}U, and ^{208}Pb/^{232}Th ratios were corrected for both instrumental mass bias and elemental and isotopic fractionation calculated using the software SILLS 1.03.0 (Murray et al. 2007). The NIST SRM 610 standard was calibrated against the Plešovice standard zircon for a spot size of 40 μm (based on the ablation and transportation behaviour of the elements we defined different ^{206}Pb/^{238}U, ^{207}Pb/^{206}Pb, ^{208}Pb/^{232}Th ratios of the NIST SRM 610 standard for 30, 40, 60 and 70 μm spot sizes); all other parameters, e.g. laser frequency (10 Hz), baseline (30 s), integration time (40 s) and energy (15 J/cm^2) were identical. Ages were calculated using ISOPLOT (Ludwig 2003) with average 2 sigma uncertainties of 2–5%.

U–Pb isotope analyses of zircons by isotope-dilution thermal ionization mass-spectrometry (ID-TIMS)

High-precision ID-TIMS (”conventional”) U–Pb zircon analyses were carried out on single zircon grains at the Institute of Isotope Geochemistry and Mineral Resources, ETH-Zurich, using an ion counter system attached to a Finnigan MAT 262 thermal ionization mass-spectrometer. Selected zircons were air- or chemically abraded (Mattinson 2005) to remove marginal zones of lead loss. They were rinsed several times with distilled water and acetone in an ultrasonic bath and washed in warm 4 N nitric acid. All single grain zircon samples were spiked with a ^{235}U–^{205}Pb mixed tracer. Total blanks were less then 0.002 ng for Pb and U. For further details see von Quadt et al. (2002). The PBDAT and ISOPLOT programs of Ludwig (1988, 2003) were used for calculating the uncertainties and correlations of U/Pb ratios. All uncertainties are reported at the 2σ level. The decay constants of Steiger and Jäger (1977) were used for age calculations, and corrections for common Pb were made using the values by Stacey and Kramers (1975).

Hf isotope analyses of zircons

Hf isotope ratios in zircons were measured on a Nu Instruments multiple collector inductively coupled plasma mass spectrometer (MC-ICPMS; David et al. 2001) at the Institute of Isotope Geochemistry and Mineral Resources, ETH Zurich. Measured ^{176}Hf/^{177}Hf values were corrected for instrumental mass fractionation using ^{179}Hf/^{177}Hf= 0.7325 (exponential law for mass bias correction). Repeated analyses of the JMC-475 standard solution during the measurement session yielded a ^{176}Hf/^{177}Hf ratio of 0.282141±14 (2 sigma). For the calculation of the ε_{Hf} values the following present-day ratios of the Chondritic Uniform Reservoir (CHUR) were used: (^{176}Hf/^{177}Hf)$_{CH}$= 0.282772 and (^{176}Lu/^{177}Hf)$_{CH}$=0.0332 (Blichert-Toft and Albarède 1997). A ^{176}Lu/^{177}Hf ratio of 0.0050 was used for age correction of the Hf isotope ratios at 90 Ma for all zircons.

The in-situ Hf isotope data were acquired using a 193 nm ArF laser connected to the Nu-500 MC-ICP-MS. Ablation was conducted in He (flow rate ~1.1 l/min) and combined with argon (~0.9 l/min) using a spot size of 40 μm and a 4 Hz laser pulse repetition rate over a 60 s ablation period. The most critical factor in obtaining accurate ^{176}Hf/^{177}Hf ratios by laser ablation concerns the ability to correct for the isobaric interference of Lu and Yb on ^{176}Hf, depending on the REE content of the analyzed zircon. The correction itself is performed by measuring an interference-free Yb isotope during the analysis, such as ^{171}Yb or ^{173}Yb, and then calculating the magnitude of the ^{176}Yb interference using the recommended ^{176}Yb/^{171}Yb or ^{176}Yb/^{173}Yb ratios of Segal et al. (2003). The Lu correction is performed in the same fashion by monitoring ^{175}Lu, and using ^{176}Lu/^{175}Lu=0.02669. To control and correct the measured Hf-ratios we analyzed four zircon standards with different REE contents (Monastery, Mud Tank, Plešovice and 91500), whose ^{176}Hf/^{177}Hf ratios were independently ascertained by analyzing the solutions that were previously purified for REE determination by chemical separation methods.

Rb–Sr and Sm–Nd whole-rock isotope analyses

The isotopic composition of Sr and Nd and the Rb, Sr, Sm and Nd contents were measured at ETH Zurich using the ID-TIMS techniques. Nd isotopic ratios were normalized to $^{146}Nd/^{144}Nd=0.7219$. Analytical reproducibility was estimated by periodically measuring the La Jolla standard (Nd) as well as the NBS 987 (Sr standard). The mean of 12 runs during this work was $^{143}Nd/^{144}Nd=0.511841\pm0.000007$ and ten runs of the NBS 987 standard yielded a $^{87}Sr/^{86}Sr$ ratio of 0.710235 ± 0.000012.

Rock chemistry and Sr and Nd characteristics

New major and trace element data are presented for the dated magmatic rocks of the Medet deposit in Table 1. They are in agreement with published data (Daieva and Chipchakova 1999; Kamenov et al. 2007): SiO_2 contents range from 59.2 wt.% in the quartz-monzodiorite (AvQ-111) to 63–65 wt.% in the granodiorite porphyries (AvQ-038 and 112) and the Q-granodiorite porphyry dyke (AvQ-210) and to 74.8 wt.% in the aplite vein. All studied rocks show a high-K calc-alkaline affinity. The REE patterns of the sampled Cretaceous rocks are characterised by enrichment in LREE and flat or slightly depleted HREE (Fig. 4a). The Eu-anomaly is absent or weak. The multi-element patterns (Fig. 4b) are characterised by depletion in Ta–Nb, enrichment in LILE and low values of HFSE, which is typical for subduction-related magmatic rocks. Discrimination diagrams of Pearce et al. (1984; Fig. 4c) and Harris et al. (1986; Fig. 4d) define a subduction-related affinity of the magmatic rocks.

These data are compared with the geochemical characteristics of the rocks from the basement (Fig. 4a, b; for sample localities see Fig. 1b). Noteworthy is the similarity

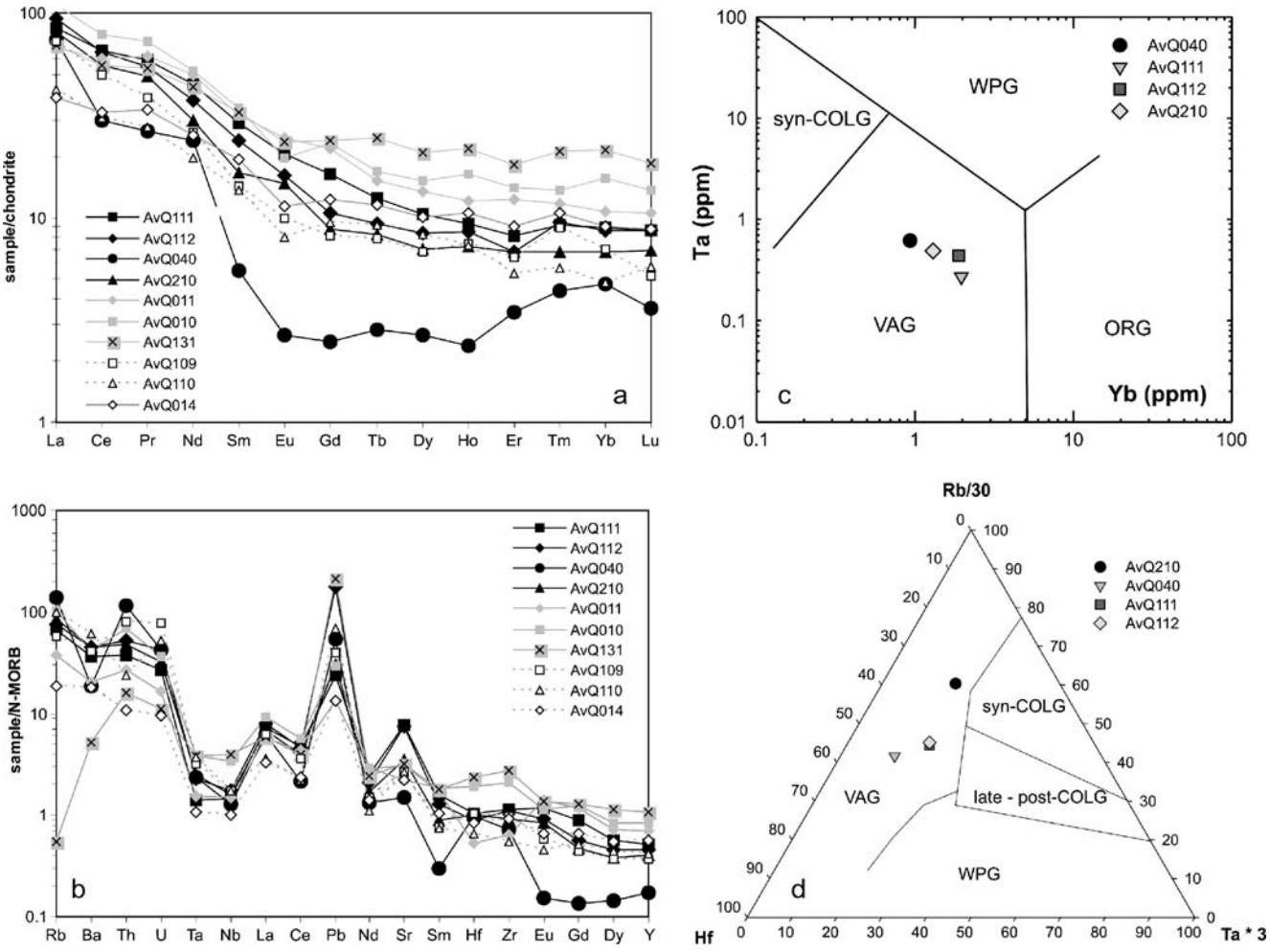

Fig. 4 Spider diagrams (**a**, **b**) and geochemical discrimination diagrams (**c**, **d**) for dated samples from the Medet deposit. **a** Chondrite-normalized REE patterns and **b** N-MORB-normalized multi-element patterns. (C1 chondrite and N-MORB values after Sun and McDonough 1989). On both diagrams data for the basement rocks are also shown (for sample numbers and description see Table 2 and text); **c** Yb–Ta diagram after Pearce et al. (1984); **d** Rb/30-Hf-Ta*3 diagram after Harris at al. (1986). *WPG* within plate granites, *COLG* collision granites, *VAG* volcanic arc granites, *ORG* ocean ridge granites

of the trace and rare-earth element distributions in the Variscan and Cretaceous magmatic rocks, whereas the trace-element contents and patterns of the metamorphic basement rocks are quite different.

Initial strontium values (corrected for a crystallization age of 90 Ma) in the magmatic rocks of the Medet deposit define a narrow range of 0.7039 (AvQ-111) to 0.7050 (AvQ-40; Table 2 and Fig. 5a). The initial strontium ratio $(^{87}Sr/^{86}Sr)_i$ does not increase significantly with increasing SiO_2 content, providing evidence for magma fractionation processes and limited contamination with crustal materials during the intrusion. The same relationship is observed between the SiO_2 content and the initial neodymium isotopic ratio $(^{143}Nd/^{144}Nd)_I$ in samples AvQ111 and AvQ038. The aplite vein (sample AvQ040, Fig. 5b), however, deviates from this trend with pronounced contamination by old continental crust.

Most rock samples lie on the mantle array of the $(^{87}Sr/^{86}Sr)_i$ vs. $(^{143}Nd/^{144}Nd)_i$ diagram (Fig. 5c) and follow the trend to the EM1 field of Zindler and Hart (1986). The aplite vein sample (AvQ040) deviates to less radiogenic (crustal influenced) $^{143}Nd/^{144}Nd$ values, whereas the basement rocks AvQ131 and AvQ010 (data are corrected for 90 Ma) diverge significantly from the mantle trend in their Sr and Nd isotope characteristics (Fig. 5c and Table 2).

U–Pb zircon dating

Q-monzodiorite (AvQ111)

Pale beige long prismatic zircons of sample AvQ111 were chosen for the dating of the Q-monzodiorite of the Medet deposit (Table 3). Two air-abraded and two non-abraded zircons with sharp edges and predominated bipyramidal faces {101} and {111}, and prismatic faces {110} yield concordant $^{206}Pb/^{238}U$ ages and define a mean of 90.36± 0.48 Ma, whereas three of them yield a weighted mean $^{206}Pb/^{238}U$ age of 90.59±0.29 Ma (Fig. 6a). The two abraded grains together determine a weighted mean $^{206}Pb/^{238}U$ age of 90.73±0.33 Ma. Five additional zircons (one air-abraded and four non-abraded) are discordant with Lower Palaeozoic inheritance. Anchoring a lower intercept age of 90.5±0.5 Ma, these zircons define an Upper intercept age of 461±10 Ma (MSWD 0.72) or 457.0± 3.5 Ma (Fig. 6b) when using only the non-abraded grains.

Granodiorite porphyries with phenocrysts of Pl and Hbl-Pl (AvQ112 and AvQ038)

Analyzed zircons from the granodiorite samples of the Medet deposit are also pale beige and prismatic. Two zircons of the Pl-granodiorite porphyry AvQ112 are

Table 2 Rb–Sr und Sm–Nd data for magmatic rocks from Medet deposit and from the basement rocks

Sample	Rock type	Rb (ppm)	Sr (ppm)	$^{87}Rb/^{86}Sr$	$^{87}Sr/^{86}Sr$	2σ error	$(^{87}Sr/^{86}Sr)_{i90}$	Sm (ppm)	Nd (ppm)	$^{147}Sm/^{144}Nd$	$^{143}Nd/^{144}Nd$	2σ error	$(^{143}Nd/^{144}Nd)_i$ at 90 Ma	ε-Nd at 90 Ma
AvQ111	Q-Monzodr	58.93	161.2	1.0570	0.705272	0.000007	0.703920	25.04	122.5	0.1233	0.512499	0.000009	0.512430	−1.79
AvQ038	Hbl-Pl-Gdr-porphyry	115	852	0.3807	0.704952	0.000009	0.704446	4.5	27	0.1667	0.512529	0.000018	0.512436	−1.68
AvQ040	Aplite vein	204.5	196.4	3.008	0.708802	0.000013	0.704955	3.34	48.8	0.0410	0.511999	0.000008	0.511976	−10.6
AvQ014	Var Medet gabbro	51.11	1,029	0.1437	0.705059	0.000020	0.704875							
AvQ110	Var Koprivshtitsa gr	125.8	303.9	1.1972	0.713624	0.000009	0.712093	3.92	13.7	0.1725	0.512299	0.000012	0.512197	−6.34
AvQ131	Pz metadiabase	2.15	158.8	0.039	0.71045	0.000024	0.71040	4.62	18.2	0.1533	0.512640	0.000015	0.512555	0.64
AvQ010	Gneiss basement	218.7	60.95	10.38	0.71770	0.00003	0.704426	1.77	7.49	0.1428	0.511991	0.000012	0.511912	−11.9

For sample numbers and description, see the text and Table 1
Monzodr monzodiorite, *Q* quartz, *Pl* plagioclase, *Hbl* hornblende, *Gdr* granodiorite, *Gr* granite, *Var* Variscan, *Pz* Palaeozoic

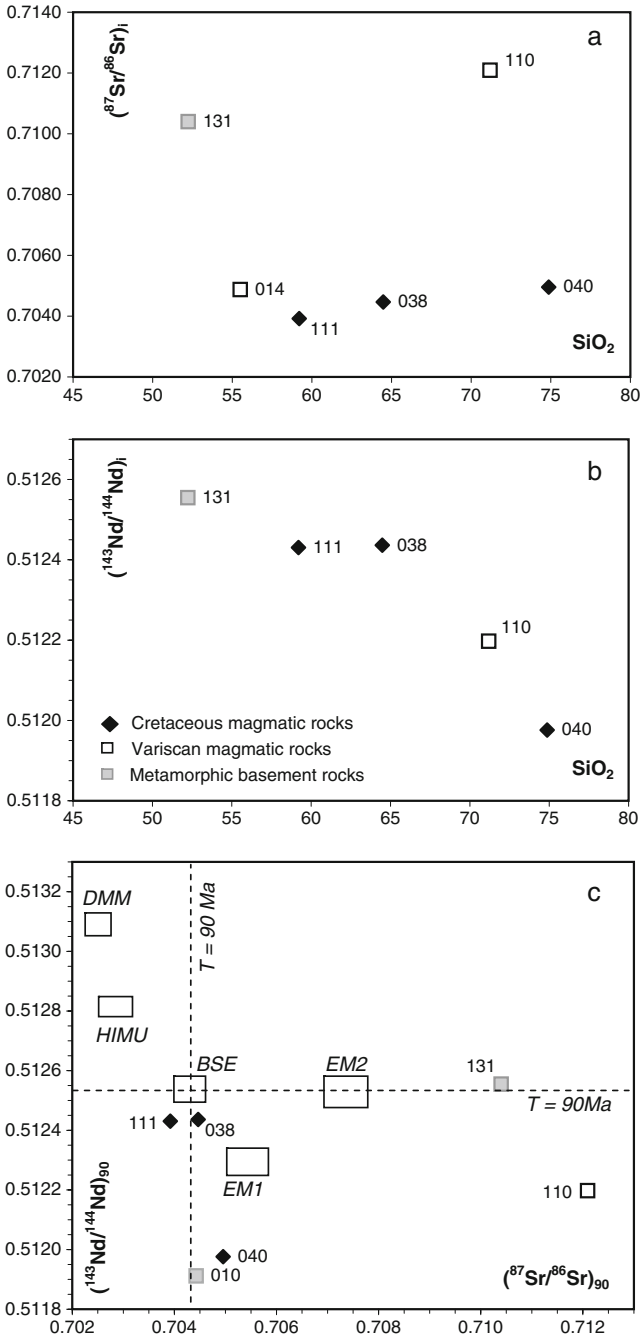

Fig. 5 Sr and Nd isotope data for whole-rock samples from the studied area (all ratios corrected for 90 Ma, see Table 2): **a** $(^{87}Sr/^{86}Sr)_i$ vs. SiO_2 and **b** $(^{143}Nd/^{144}Nd)_i$ vs. SiO_2 diagrams; **c** $(^{87}Sr/^{86}Sr)_i$ vs. $(^{143}Nd/^{144}Nd)_i$ diagram. Fields of DMM (depleted MORB mantle), HIMU (magma source having a high μ—$^{238}U/^{204}Pb$ ratio), EM1 and 2 (enriched mantle) and BSE (bulk silicate earth) are given according to Zindler and Hart (1986) and Hart and Zindler (1989). *Dashed lines* correspond to the Sr and Nd isotope values of the undifferentiated reservoir—identical to CHUR (DePaolo 1988; Faure 2001), corrected for 90 Ma. For sample numbers and description see Table 1 and the text. The legend for the used symbols is shown on **b**

concordant at 90.47±0.30 Ma (Table 3, Fig. 6c) whereas one is slightly discordant and reveals lead loss.

Zircons from the Hbl-Pl granodiorite porphyry (AvQ038) reveal lead inheritance likely related to inherited cores (Table 3), as well as lead loss. Only three of the measured zircons (pale beige, with sharp edges) are without inheritance and define a concordia age of 90.31±0.63 Ma (calculated using the two zircons with the best concordance, Fig. 6d). Using this age as the crystallization age, a discordia can be anchored from this point through the zircons with inheritance. The discordia is not well defined, but points to a Lower Palaeozoic source for the inherited materials (500–580 Ma).

Aplite vein (AvQ040)

The age of the aplite vein (AvQ040) is important, as it cross cuts the Hbl-Pl granodiorite porphyry (AvQ038), whose age is somewhat imprecise. Some of the zircons (pale beige, prismatic) from the aplite vein also yield evidence of inheritance, but two zircons are concordant at 90.12±0.36 Ma (Fig. 6e). The inheritance reveals a similar Lower Palaeozoic age (upper intercept age of the discordia at about 550 Ma) as in the zircons of the Hbl-Pl granodiorite porphyry AvQ038.

Granodiorite porphyry dyke (AvQ210)

Only prismatic and long prismatic zircons of the dyke were chosen for dating. As commonly observed in dyke samples, the zircons reveal lead inheritance and lead loss (Table 3). The inheritance is observed mostly in the chemically abraded (Mattinson 2005) grains and is related to materials of Variscan age (Table 3). A possible candidate for the Variscan inheritance could be the Koprivshtitsa granite, into which the dyke is emplaced. Two air-abraded pale beige zircons with sharp edges from the smallest size fraction are concordant at 89.26±0.32 Ma, and two non-abraded grains yield the same $^{206}Pb/^{238}U$ age, but a slightly discordant $^{207}Pb/^{235}U$ age. The weighted mean $^{206}Pb/^{238}U$ age of all four zircons is calculated to be 89.30±0.21 Ma (Fig. 6f).

Hf-isotope and geochemical zircon tracing

Hf-isotope characteristics of the zircons

Hf isotope studies were used to provide geochemical information for the dated zircons. The ε-Hf values are corrected for the corresponding age determined by the U–Pb method (Table 3). The initial ε-Hf values (corrected for 90 Ma) of the Upper Cretaceous zircons range from −3.59 to +5.41 (Table 4 and Fig. 7) whereas the majority lying in

Table 3 U–Pb zircon ID-TIMS isotope data for magmatic rocks from Medet deposit

N	Analysis number	Size fraction, μm	Weight in mg	Zircon description	U ppm	Pb ppm	$^{206}Pb/^{204}Pb$	$^{206}Pb/^{238}U$	2σ error %	$^{207}Pb/^{235}U$	2σ error %	$^{207}Pb/^{206}Pb$	2σ error %	$^{206}Pb/^{238}U$ apparent ages	$^{207}Pb/^{235}U$ apparent ages	$^{207}Pb/^{206}Pb$ apparent ages	Rho
Q-monzodiorite (AvQ111)																	
1	IP210	−100+75	0.0111	prism beige abr	39.82	0.700	356.6	0.014139	0.52	0.095424	1.67	0.048948	1.51	90.5	92.5	145.3	0.45
2	IP211	−100+75	0.0057	prism beige abr	117.2	8.689	2089	0.069449	0.49	0.539418	0.56	0.056332	0.25	433	438	465	0.90
3	IP212	−100+75	0.0074	prism beige abr	36.80	0.803	154.7	0.014211	0.53	0.099680	2.21	0.050873	2.03	91.0	96.5	235	0.45
4	IP211	−150+100	0.0420	prism beige	20.64	2.498	98.54	0.066465	0.73	0.499588	4.78	0.054515	4.44	421	411	392	0.52
5	IP214	−100+75	0.0076	prism beige	65.64	1.197	284.4	0.014035	0.49	0.092613	1.4	0.047857	1.24	89.8	89.9	92.2	0.47
6	IP215	−100+75	0.0175	prism beige	29.09	0.530	269.2	0.014077	0.68	0.097992	7.04	0.050486	6.62	90.1	94.9	217	0.65
7	IP216	−100+75	0.0068	prism beige	196.9	8.405	1963	0.041564	0.46	0.312847	0.50	0.05459	0.18	262	276	396	0.93
8	IP217	−150+100	0.0469	prism beige	56.58	2.903	4573	0.049567	0.48	0.377207	0.50	0.055194	0.15	312	325	420	0.96
9	IP218	−100+75	0.0089	prism beige	419.1	26.69	730.4	0.062952	2.54	0.482396	2.56	0.055576	0.24	394	400	435	0.99
Pl-granodiorite porphyry (AvQ112)																	
1	112-1	−100+75	0.0063	long prism pale beige	143.3	3.271	116.1	0.013645	0.83	0.090835	6.2	0.048282	6.2	87.36	88.28	113.1	0.42
2	112-3	−100+75	0.0094	long prism beige abr	118.2	2.205	225.7	0.014121	0.46	0.093136	0.59	0.047833	0.37	90.39	90.42	91.04	0.78
3	112-2	−100+75	0.0055	long prism beige abr	78.88	1.522	214.8	0.014143	0.46	0.093314	0.61	0.047849	0.38	90.54	90.59	91.84	0.77
Hbl-Pl-granodiorite porphyry (AvQ038)																	
1	038/1	−100+75	0.0226	long prism beige	93.79	1.482	1329	0.013969	0.51	0.092644	1.01	0.048102	0.82	89.42	89.96	104.28	0.58
2	038/2	−100+75	0.0120	long prism beige	173.3	2.692	1251	0.014027	0.48	0.092796	0.71	0.047981	0.50	89.80	90.10	98.31	0.71
3	038/3	−100+75	0.0222	long prism beige	107.3	2.128	2486	0.018970	0.54	0.134055	1.00	0.051252	0.80	121.1	127.7	252.2	0.60
4	038/4	−100+75	0.0056	long prism beige abr	156.3	3.274	177.4	0.015118	0.46	0.099734	0.72	0.047847	0.52	96.7	96.5	91.7	0.69
5	038/5	−100+75	0.0146	long prism beige abr	140.8	2.289	850.8	0.014165	0.47	0.093606	0.50	0.047929	0.18	90.67	90.86	95.78	0.93
6	2771	−100+75	0.0047	long prism beige	354.3	5.863	1019	0.015253	0.78	0.103121	1.27	0.049032	0.97	97.58	99.65	149	0.64
7	2772	−100+75	0.0055	long prism beige	68.33	1.328	206.8	0.013851	0.68	0.099337	5.12	0.052015	4.82	88.67	96.16	286	0.49
Aplitic vein (AvQ040)																	
1	0037	−100+75	0.0048	long prism beige	133.5	3.348	102.28	0.014083	0.52	0.091230	3.72	0.046984	3.5	90.15	88.65	48.43	0.48
2	0038	−100+75	0.0065	long prism beige	143.2	3.743	236.7	0.019981	0.49	0.142336	2.27	0.051664	2.09	127.5	135.1	270.6	0.45
3	0039	−100+75	0.0047	long prism beige	175.5	5.225	75.86	0.014027	0.68	0.089521	4.78	0.046286	4.50	89.79	87.05	12.55	0.47

Q-granodiorite porphyry (AvQ210)																
1	210/1	−100+75	0.0068	prism beige abr	15.82	0.344	125.9	0.013942	0.48	0.094005	1.3	0.048900	1.14	89.3	91.2	143	0.49
2	210/2	−100+75	0.0042	prism beige abr	69.10	1.044	660	0.013747	0.48	0.091366	0.57	0.048204	0.28	88.0	88.8	109	0.86
3	210/3	−100+75	0.005	prism beige abr	24.83	0.474	231	0.013940	0.48	0.093993	0.75	0.048901	0.55	89.2	91.2	143	0.68
4	210/4	−75+63	0.0029	prism beige	8.19	0.237	73.67	0.013958	0.52	0.094212	3.3	0.048955	3.1	89.4	91.4	146	0.45
5	210/5	−75+63	0.0026	prism beige	23.7	0.488	174.3	0.013948	0.47	0.092988	1.15	0.048352	1.0	89.3	90.3	116	0.51
6	3001	−150+100	0.0217	long prism beige	77.61	1.261	548	0.01413	0.56	0.09398	0.82	0.048249	0.58	90.4	91.2	112	0.70
7	3008	−150+100	0.0274	long prism beige, CA	73.40	1.599	717.7	0.01935	0.73	0.13186	0.77	0.049424	0.28	124	126	168	0.95
8	3011	−150+100	0.0125	long prism beige, CA	71.37	3.236	183.6	0.03506	0.70	0.25870	1.2	0.053522	0.95	222	234	351	0.62
9	3046	−150+100	0.0131	long prism beige, CA	59.63	1.484	397.9	0.02456	1.02	0.17416	1.8	0.051426	1.41	156	163	260	0.63

Rho correlation coefficient $^{206}Pb/^{238}U$–$^{207}Pb/^{235}U$
abr abraded, *CA* chemical abrasion, *prism* prismatic

the range of −1 to +3. These values are typical for mixed mantle–crust sources of the magma. Zircons of the Q-monzodiorite (AvQ111) reveal the most homogeneous ε-Hf values (in a narrow range from +1.4 to −0.9), which is characteristic for zircons that crystallized from a homogeneous magma. In the same sample, inherited zircon grains and cores of Lower Paleozoic age (456.5±5.5 Ma, Fig. 6b) reveal also mixed, but mantle-dominated origin (460 Ma corrected ε-Hf values of +6.3 to +8.1, Table 4). Furthermore, the 90 Ma-corrected ε-Hf values of the newly saturated Turonian zircons and the inherited grains/cores do not differ significantly, possibly inferring a significant contribution of the Lower Palaeozoic materials to the generation of the Cretaceous magma, prior to their intrusion in the upper continental crust. Zircon contamination with Variscan materials was negligible (detected only in one grain by in-situ LA-ICP-MS dating, Table 5).

Similar features are also observed in the zircons of the Hbl-Pl granodiorite porphyry (AvQ038, Table 4 and Fig. 7), although the range of the ε-Hf (90 Ma) values is wider. In the aplite vein (AvQ040), however, the inherited zircon grains exhibit more crustal dominated values and suggest an additional source in the upper continental crust (one zircon core with an age of >700 Ma reveals a ε-Hf (90 Ma) value of −40.6). The tendency towards a wider range of the ε-Hf values is preserved in the later Q-granodiorite porphyry dyke (AvQ210, Table 4). In the aplite vein and in the dyke, the latest products of the magmatic activity of the Medet deposit, the newly saturated zircons consistently reveal a more mantle dominated source component (from +1.8 to +3.5 in AvQ040 and from +3 to +5 in the dyke AvQ210), and only contamination with upper crustal materials results in negative ε-Hf values. There, the fast cooling possibly did not allow homogenization of the two sources prior to crystallization of the zircons.

CL/ BSE images and trace/rare earth element distribution of the zircons

CL and BSE images were used to investigate the internal textures of the zircons from the different magmatic rocks. The studied zircons show typical CL/BSE images for intermediate to acid rocks: fine oscillatory zoning patterns (OZPs) and rarely sector zoning (Fig. 8). Only in one zircon of the most basic sample, the Q-monzodiorite, we observe widely spaced OZPs in the central part, which is a characteristic feature for a low degree of zircon saturation (Vavra 1990). Light zones in the BSE images or dark ones in CL (rich in heavy elements like U and Th) are usually uniformly distributed and not concentrated in the outer parts as expected in an evolving differentiated magma. Inherited zircons and inclusions are easily distinguished when present.

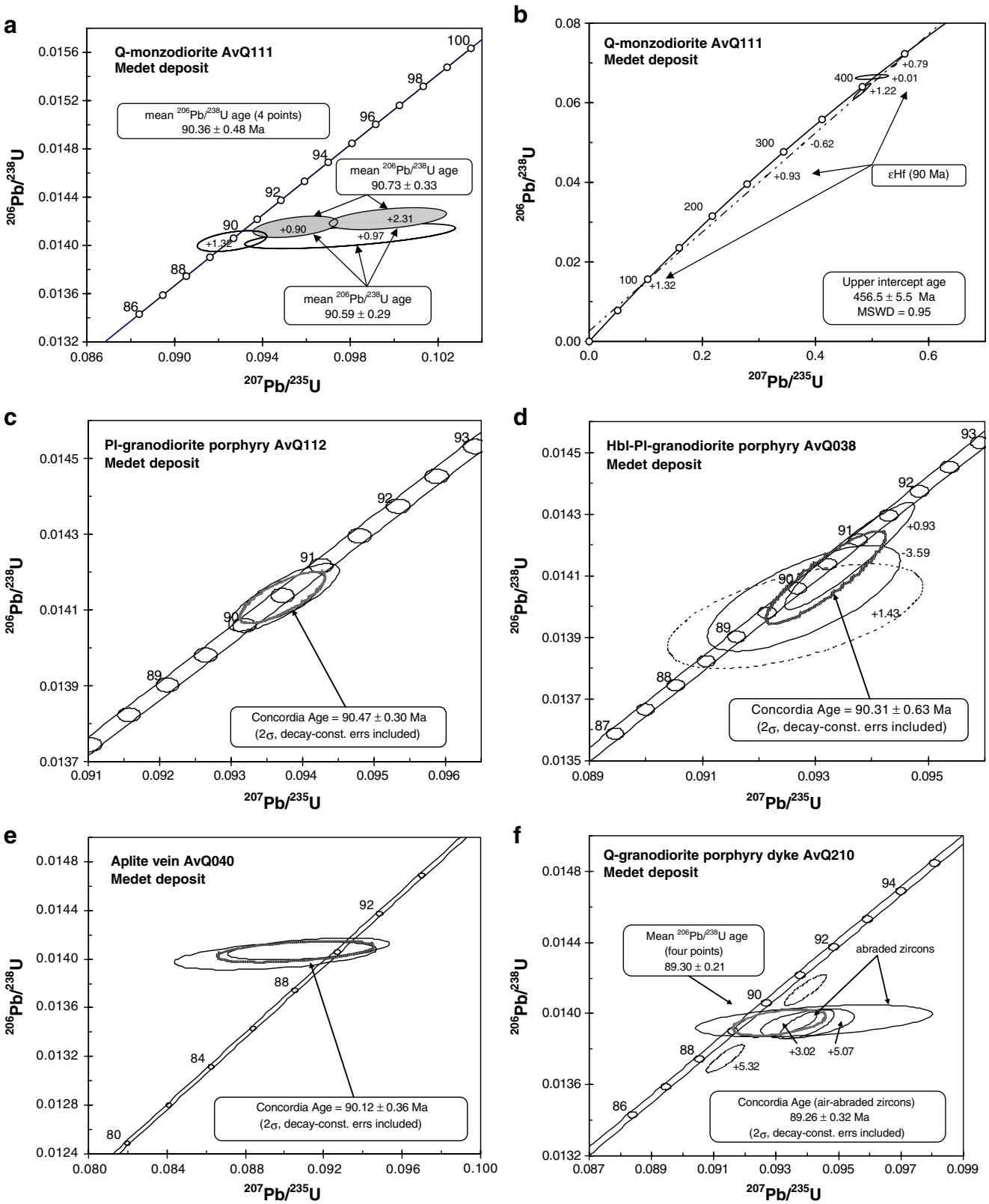

Fig. 6 U–Pb concordia diagrams for single grain zircon analyses of samples AvQ111 (**a**, **b**), AvQ112 (**c**), AvQ038 (**d**), AvQ040 (**e**) and AvQ210 (**f**). The εHf data of Table 4 are plotted alongside the corresponding age *ellipse*

Table 4 Hf isotope data for zircons from the magmatic rocks in the Medet deposit, Central Srednogorie

Sample *N*	Lab. *N*	Age (Ma)	$^{176}Hf/^{177}Hf$	2 σ error	ε Hf today	ε Hf T 90 Ma	ε Hf T 460 Ma
Single zircon MC-ICP-MS (on TIMS-dated zircons)							
AvQ038	038/1	90	0.282765	0.000029	−0.25	1.43	
	038/2	90	0.282623	0.000036	−5.27	−3.59	
	038/3	Core 500	0.282855	0.000008	2.94	4.61	11.54
	038/4	s core	0.282650	0.000023	−4.31	−2.64	
	038/5	90	0.282751	0.000008	−0.74	0.93	
	2772	90	0.282812	0.000009	1.41	3.09	
	2771	s core to 500	0.282784	0.000003	0.42	2.10	9.03
AvQ111	IP210	90	0.282750	0.000008	−0.78	0.90	
	IP211	469	0.282747	0.000006	−0.88	0.79	7.72
	IP212	90	0.282790	0.000009	0.64	2.31	
	IP213	460	0.282725	0.000005	−1.66	0.01	6.94
	IP214	90	0.282762	0.000011	−0.35	1.32	
	IP215	90	0.282752	0.000005	−0.71	0.97	
	IP216	460core	0.282751	0.000005	−0.74	0.93	7.86
	IP217	460core	0.282707	0.000003	−2.30	−0.62	6.30
	IP218	460	0.282759	0.000004	−0.46	1.22	8.14
AvQ210	3308	s core to 460	0.282655	0.000004	−4.14	−2.46	4.08
	210-1	90	0.282868	0.000012	3.39	5.07	
	210-2	90	0.282875	0.000016	3.64	5.32	
	210-3	90	0.282810	0.000010	1.34	3.02	
In-situ Laser-ablation MC-ICP-MS							
AvQ210	210-13	90	0.282704	0.00005	−0.73	3.19	
AvQ040	040-1	~90	0.282783	0.000016	0.42	2.31	
	040-2	~90	0.282771	0.000016	0.00	1.85	
	040-5	~90	0.282816	0.000027	1.59	3.47	
	040-7	~90	0.282796	0.000028	0.88	2.75	
	040-8	~90	0.282709	0.000024	−2.19	−0.33	
	040-9	Rim ~90	0.282815	0.000025	1.56	3.43	
	040-9	Core >700	0.281571	0.000025	−42.44	−40.56	
AvQ112	112-1	~90	0.282770	0.000024	−0.05	1.82	
	112-2	~90	0.282804	0.000025	1.17	3.01	
	112-3	~90	0.282737	0.000016	−1.20	0.67	
	112-4	~90	0.282787	0.000017	0.57	2.44	
	112-5	~90	0.282771	0.000016	0.00	0.57	
	112-7	~90	0.282871	0.000021	3.54	5.41	
	112-8	~90	0.282707	0.000023	−2.28	−0.43	

Numbers of the conventionally dated zircons are as in Table 3 (samples AvQ038, AvQ111, and AvQ210). Samples AvQ112, AvQ040 and AvQ210 were analyzed by in situ MC-LA-ICP-MS method and the corresponding in situ $^{206}Pb/^{238}U$ age is given in the "age" column
s small

All Upper Cretaceous zircons yielded similar REE patterns. The intermediate and heavy rare earth elements (REE) reveal a constant and typical magmatic pattern (Hoskin and Ireland 2000; Belousova et al. 2002) with a steep enrichment in HREE (Fig. 8). Positive Ce anomalies were found in all analyzed grains (Table 5). The reason for this anomaly is that under oxidizing conditions, Ce can be present in both the 4^+ and 3^+ valence states. In general, 4^+ cations are significantly more soluble in zircon than 3^+ cations because their incorporation into the Zr^{4+} site does not require any charge balancing, and Ce^{4+} is closer in size to Zr^{4+} than Ce^{3+} (e.g. Belousova et al. 2002; Hoskin and Schaltegger 2003 and references therein). The Ce/Ce* ratio (calculated as $Ce/\sqrt{(La \times Pr)}$) in the magmatic zircons from Medet not only varies from sample to sample, but also among the zircons from one sample (AvQ040, Fig. 9a). A tendency towards slightly increasing positive Ce-anomaly is observed in the temporal succession of magmatic rock units from the Q-monzodiorite (AvQ111) to the Pl- and Hbl-Pl granodiorite porphyries and the aplitic vein. This suggests an increase in the oxygen fugacity. The late granodioritic dyke is distinguished by its lower Ce/Ce* ratio, hence lower oxygen fugacity.

Another indicator of the oxygen fugacity in the zircons is the Eu/Eu* ratio ($Eu/\sqrt{(Sm \times Gd)}$. Under oxidizing magma conditions all Eu is trivalent, therefore the resulting

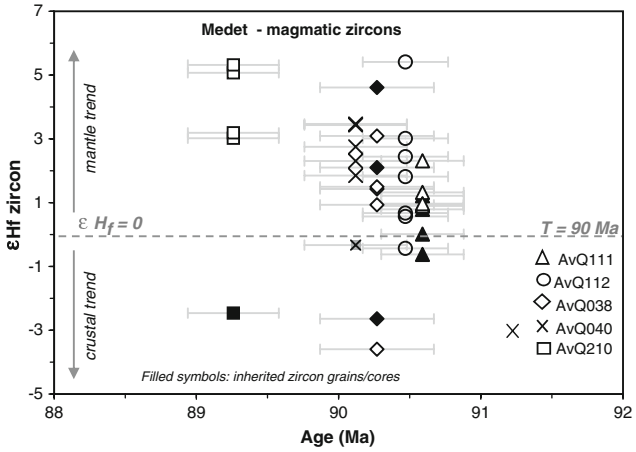

Fig. 7 Variation of εHf (t) zircon data in the studied rock samples from Medet deposit. *Filled symbols* indicate inherited zircon grains and cores. The *grey line* shows the zero εHf value of the Chondritic Uniform Reservoir (CHUR)

Fig. 8 Cathodoluminescence (CL) images of zircons from samples **a** AvQ111, **b** AvQ112, **c** AvQ038 and **d** AvQ040 with the corresponding chondrite-normalized distribution of the REE (*R* rim, *C* core). *Circles on the pictures* correspond to the laser ablation spot (from the LA-ICP-MS analyses) in the zircon crystals, and *numbers*—to the calculated $^{206}Pb/^{238}U$ age (2σ errors are ~2–5% for the analyses with a 40 μm spot size, and 6–15% for that with a 20 μm spot size)

normalized zircon REE pattern should not have an Eu-anomaly (Eu/Eu* ratio of 1.0), whereas under less oxidized conditions the larger Eu^{2+} ion does not substitute for the considerably smaller Zr^{4+} resulting in a negative Eu-anomaly (Hoskin and Schaltegger 2003 and references therein). The effect of the oxidizing conditions on the Eu-anomaly within the zircons is similar to the effect of plagioclase fractionation in the magma. However, the magmatic whole rock samples of the Medet deposit show only a weak Eu-anomaly (Fig. 4a, b), consequently the interpretations of the Eu/Eu* ratio can be related to the oxidation state of the magma. On the Eu/Eu* vs. age diagram (Fig. 9b) first the Eu/Eu* ratio (and also the oxygen fugacity) increases from the Q-monzodiorite (AvQ111) to the Pl- and Hbl-Pl granodiorite porphyries and to the aplite vein, and it then decreases in the late Q-granodiorite porphyry.

Trace elements concentrations as well as indicative ratios such as Nb/Ta in the analyzed zircons from Medet deposit are also used for magma source characterization. The Nb/Ta ratios generally range from 5 to 10 in all magmatic zircons, except the Q-granodiorite porphyry dyke (Fig. 9c), where it is about 3. The influence of the continental crust in sample AvQ210 is also visible on a diagram showing the Y content (Fig. 9d). The very similar characteristics of the zircons from the Q-monzodiorite, the Pl- and Hbl-Pl granodiorite porphyries and the aplitic vein on the diagrams of Y vs. Hf and ∑REE (Fig. 10a, b) argue for a common upper crustal chamber. However, Th and U seem to be more closely related to the whole rock chemistry and the differentiation of the magma (Fig. 10c, d), but not only to crustal assimilation. Figure 10a–d demonstrate the influence of the assimilated materials on the characteristics of the Cretaceous magmatic rocks. It shows that the Upper Cretaceous magma was contaminated with inherited zircons (filled symbols) of different origin (crustal, mantle or mixed). The sum of the REE and the Y content change linearly in the studied zircons (Fig. 10b). The increase in value corresponds to higher contribution of continental crust components in the magma and is marked mainly by some inherited zircons and by a few Cretaceous zircons of the later dyke (AvQ210).

Discussion

Timing of the ore-related magmatism in the Medet deposit

The precise U–Pb-zircon dating of the magmatism in the Medet deposit demonstrates that the entire period of the ore-related magmatism is less than 1.12 Ma. The age data are in agreement with the field observations for the time-succession of the dykes in the Medet deposit. Fertile magmatism started at 90.59±0.29 Ma (or 90.36±0.48 Ma) with the intrusion of the Q-monzodiorite porphyry (AvQ111, Fig. 11) and the Pl-granodiorite porphyry (AvQ112) at 90.47±0.30 Ma, followed by the Hbl-Pl granodiorite porphyry (AvQ038) at 90.27±0.60 Ma and finishing with the cross-cutting aplite veins with an age of 90.12±0.36 Ma (AvQ040). All these rocks are overprinted by the K-silicate alteration and host the economic mineralization. The magmatic–hydrothermal system responsible for the main high-temperature Cu–(Mo) porphyry deposition at Medet presumably ceased after about 90.12±0.36 Ma (Fig. 11). The later Q-granodiorite porphyry dyke (AvQ210) with an age of 89.26±0.32 Ma crosscuts the Upper Cretaceous units described above. It is overprinted by propylitic alteration and only contains low-temperature quartz–pyrite mineralization (280–240°C; Strashimirov and Kovachev 1992) and possibly also quartz–galena–sphalerite mineralization of non-economic grade.

Multiple magma intrusions are responsible for the rather long-lived magmatic–hydrothermal system, compared with the estimated time for one single magma/dyke emplacement and hydrothermal mineralization event of 10,000 to 200,000 years (Cathles et al. 1997; Marsh et al. 1997). The multiple intrusions of fertile magma could explain the observations of Chipchakova (2002) who distinguished two

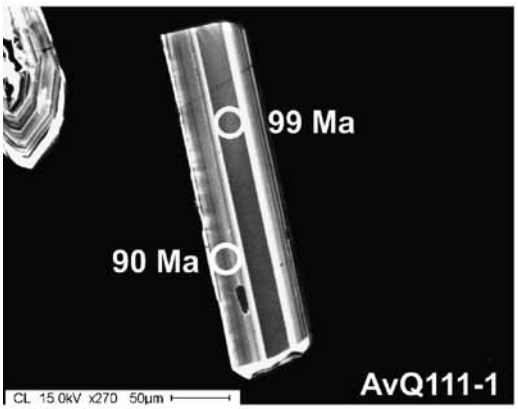
99 Ma
90 Ma
AvQ111-1
CL 15.0kV x270 50µm

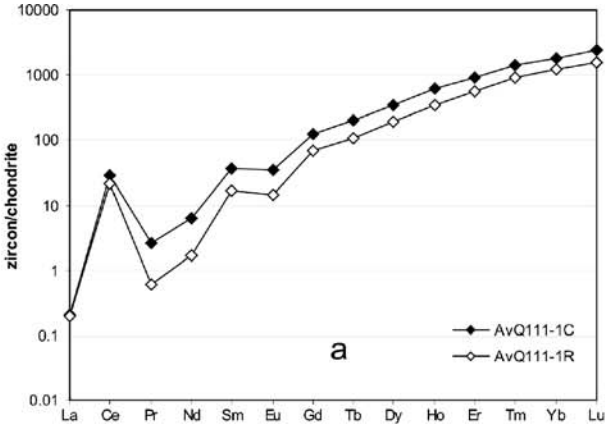
zircon/chondrite
10000
1000
100
10
1
0.1
0.01
La Ce Pr Nd Sm Eu Gd Tb Dy Ho Er Tm Yb Lu
AvQ111-1C
AvQ111-1R
a

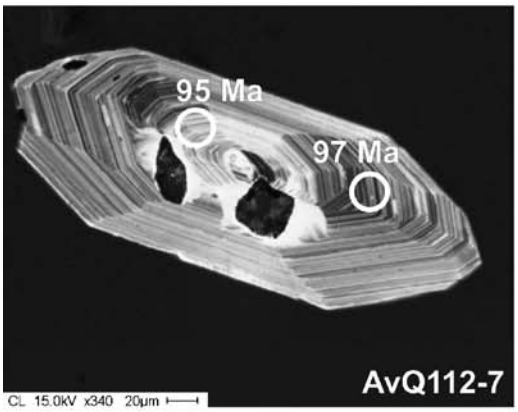
95 Ma
97 Ma
AvQ112-7
CL 15.0kV x340 20µm

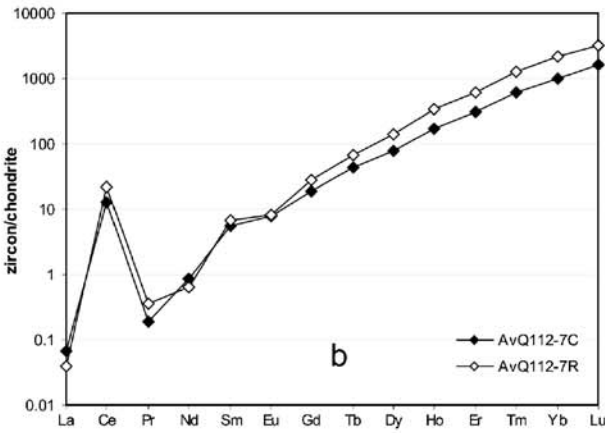
zircon/chondrite
10000
1000
100
10
1
0.1
0.01
La Ce Pr Nd Sm Eu Gd Tb Dy Ho Er Tm Yb Lu
AvQ112-7C
AvQ112-7R
b

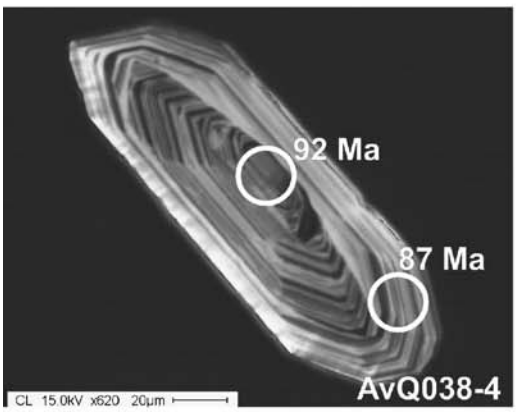
92 Ma
87 Ma
AvQ038-4
CL 15.0kV x620 20µm

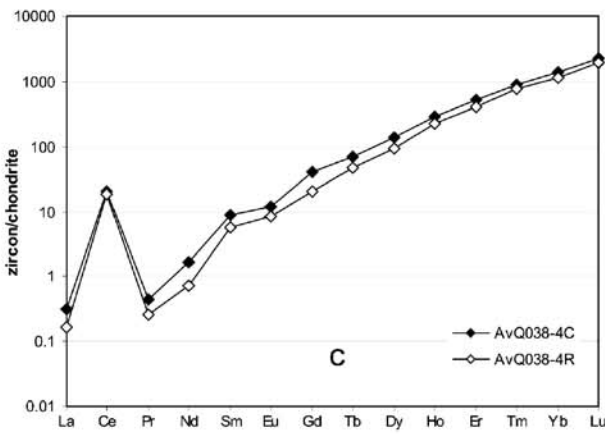
zircon/chondrite
10000
1000
100
10
1
0.1
0.01
La Ce Pr Nd Sm Eu Gd Tb Dy Ho Er Tm Yb Lu
AvQ038-4C
AvQ038-4R
c

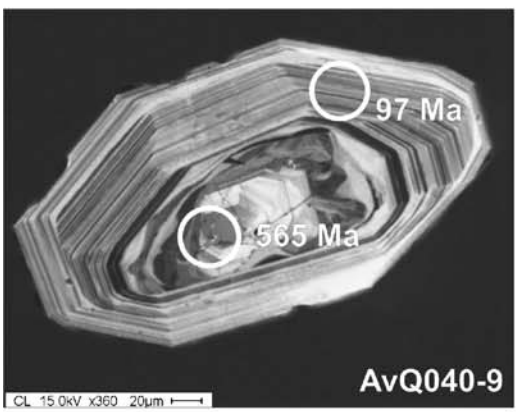
97 Ma
565 Ma
AvQ040-9
CL 15.0kV x360 20µm

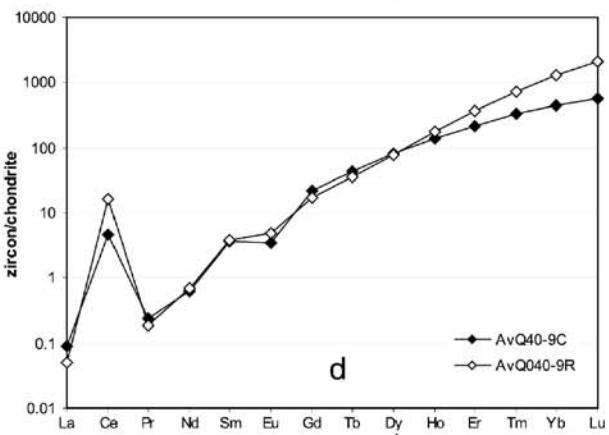
zircon/chondrite
10000
1000
100
10
1
0.1
0.01
La Ce Pr Nd Sm Eu Gd Tb Dy Ho Er Tm Yb Lu
AvQ40-9C
AvQ040-9R
d

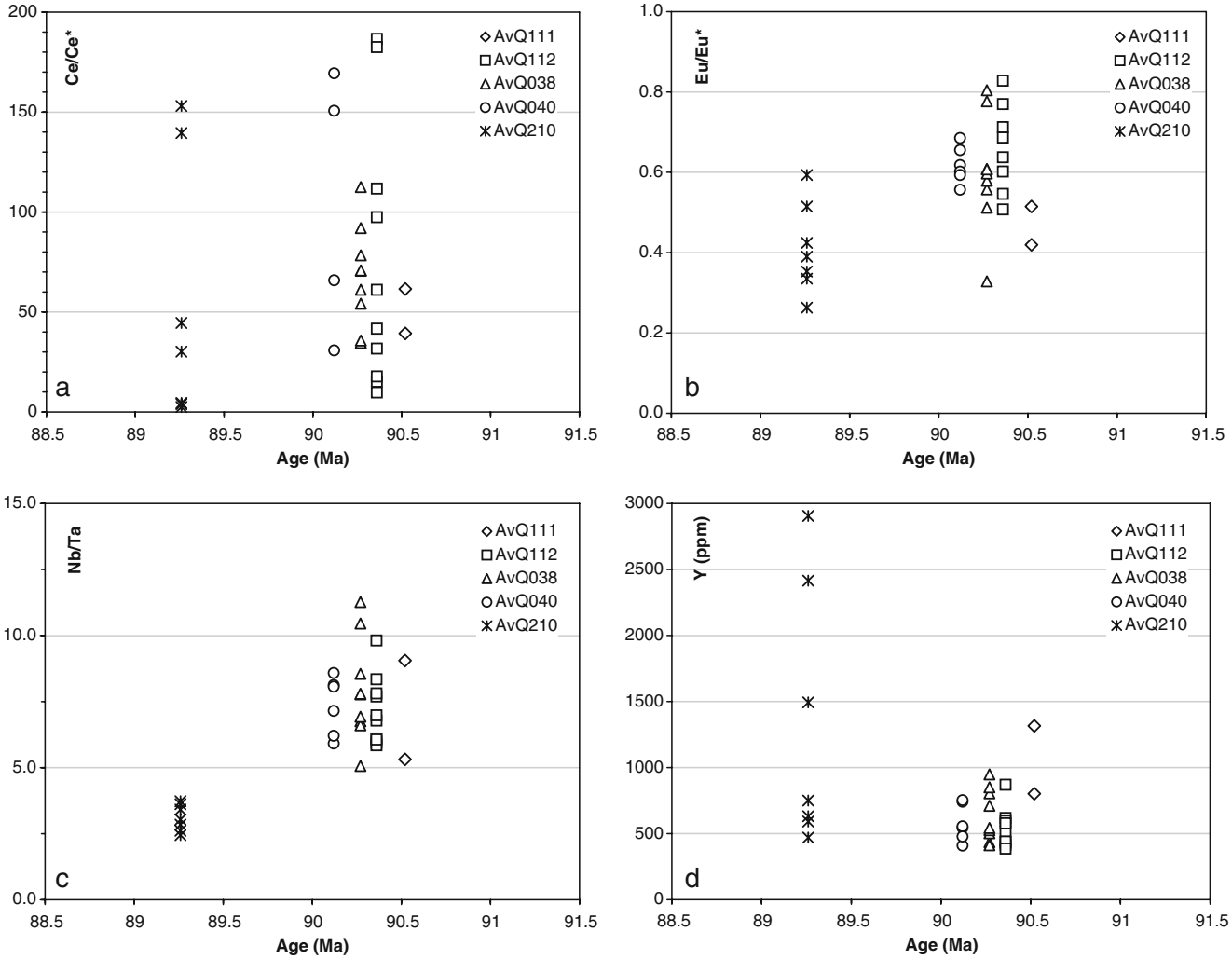

Fig. 9 Variations of Ce/Ce* (**a**), Eu/Eu* (**b**), Nb/Ta ratio (**c**) and Y content (ppm) in Upper Cretaceous zircons (or zircon domains—rim or core) from studied samples of the Medet deposit

main Cu–(Mo) mineralization phases at Medet as well biotite-forming alteration phases (Chipchakova 2002).

A summary diagram for the timing of magmatism and hydrothermal mineralization and alteration in the Medet deposit is presented in Fig. 11. Only the U–Pb zircon dating and the Re–Os dating of molybdenite (Zimmerman et al. 2008) offer a comparably robust and precise ages for the high-temperature mineralizing events. The K–Ar and $^{40}Ar/^{39}Ar$ isotope data for the Medet deposit show considerable scatter: 90.4±0.9 Ma (Lips et al. 2004), 88–86 Ma (Lilov and Chipchkova 1999; Handler et al. 2004), and 79 Ma (Lilov and Chipchkova 1999; Lips et al. 2004; Fig. 11). Both systems provide evidence for the cooling history of the region. Ages of 88–86 Ma can be explained by protracted cooling, after the collapse of the main hydrothermal system. However, such an interpretation is not adequate for the sericite age of 79 Ma. It is more feasible that one or more low-temperature (~100–200°C) reheating events occurred after emplacement of the porphyritic intrusions. The influx of deep-seated magma may have caused the development of late low-temperature hydrothermal alteration assemblages at the Medet deposit, contemporaneous to the gabbro intrusions, some 15–30 km away (at about 86 Ma in Elshitsa and 82 and 79 Ma in Velichkovo and Capitan Dimitrievo, respectively, e.g. Peytcheva et al. 2008). A similar scenario was suggested by Harris et al. (2008) for the hydrothermal system of the Bajo de la Alumbrera deposit, Argentina, but may be common in many subduction-related ore deposits worldwide.

Sources and evolution of the magma

Whole rock isotope-geochemical features of the magmatic rocks in the Medet deposit define a subduction-related tectonic setting and a mixed crust–mantle origin for the Upper Cretaceous magma (Figs. 4 and 5). The conventional

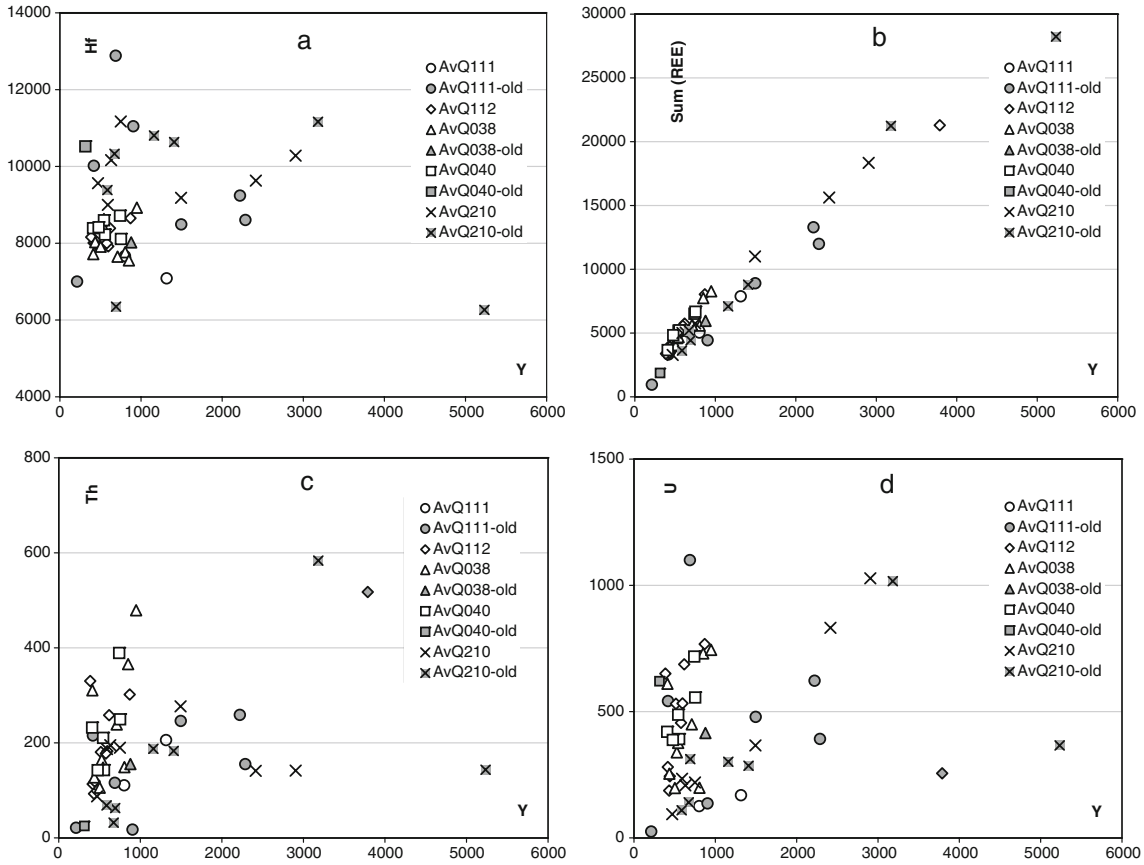

Fig. 10 Evolution of **a** Hf, **b** Sum(REE), **c** Th and **d** U content in newly crystallized and inherited zircons of the studied samples from Medet deposit. The respective elements are plotted vs. *Y*

and in-situ Hf- and trace/REE LA-ICP-MS data for the zircons from the studied rocks, combined with the age-data of the same grains provide information for the characteristics of both—the mantle and the crustal source. The Cretaceous zircons reveal ε-Hf values mainly in the range of 0 to +3, although few of them range from +5 to −1 (Fig. 7 and Table 4). These values are considerably lower, than the ε-Hf characteristics of the hybrid gabbros from the southern parts of Central Srednogorie (+8 to +10, Peytcheva et al. 2008), the latter belong to the most primitive magma in Central Srednogorie (see also the summary of Kamenov et al. 2007). Therefore, for the Cretaceous magmas of the Medet deposit an additional crustal component is needed, which was assimilated prior to zircon saturation and crystallization. As we can see from the in-situ dating of the zircons (Table 5), some grains and their cores can be related to magma contamination during the ascent and crystallization of the Cretaceous magma. Supporting evidence for this conclusions are the inherited-core ages of around 500–700 Ma and around 300–340 Ma that can be related to the basement of the Cretaceous dykes and bodies; metamorphic zircons with an age of 500–700 Ma and Variscan metamorphic rocks and granitoids were reported by Carrigan et al. (2006) and Peytcheva and von Quadt (2004). A specific characteristic of the Medet magma was the assimilation of Lower Paleozoic materials, which were themselves of mantle to mixed mantle–crust origin. The inherited ~460 Ma old zircons are widespread in the Q-monzodiorite (AvQ111) and

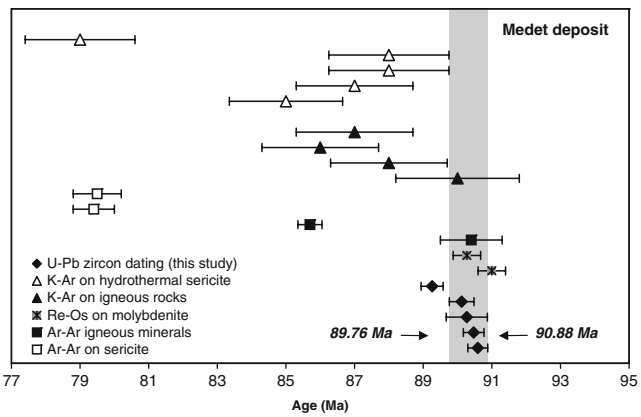

Fig. 11 Summary diagram for the timing of magmatism and mineralization in the Medet deposit, including the ID-TIMS U–Pb dating of single magmatic zircons from this study, as well as published K–Ar (Lilov and Chipchkova 1999) and Ar–Ar data (Lips et al. 2004; Handler et al. 2004) for whole rock samples, magmatic and hydrothermal minerals and Re–Os data for molybdenite (Zimmerman et al. 2008)

show ε-Hf values of +6 to +8 (corrected for 460 Ma). Noteworthy, these zircons have the same ε-Hf characteristics at 90 Ma (0 to +2, Fig. 7 and Table 4), as the majority of the newly saturated Cretaceous zircons. Consequently, Lower Paleozoic rocks may have contributed significantly to formation of the Cretaceous magma in the lower-crust—in the zone of intensive "melting, assimilation, storage, and homogenization"—the MASH zone (e.g. Hildreth and Moorbath 1988). Homogenized magmas generated in the MASH zone were emplaced in the upper crust to form the magma chamber below the Medet deposit (geophysical data of Tsvetkov et al. 1978). During the magma ascent and storage in the upper crustal chamber, this magma was further fractionated and additionally contaminated by the basement rocks.

The scenario that we constrained from the age and Hf-zircon isotope data is largely supported by the trace element distribution of the zircons and by the characteristic mineral assemblages of the Medet deposit. As mentioned above the main economic quartz–pyrite–chalcopyrite association is accompanied by specific Co–Ni assemblages, rare Cu–Sn–V and Bi–Ag–Te assemblages (Strashimirov et al. 2002) and traces of PGE-minerals (Tarkian and Stribrny 1999). PGE, Co, Ni and V are common in basic/ultrabasic rocks, rather than in calc-alkaline intermediate rocks. A potential source for them would be the Lower Paleozoic rocks with mantle signature. The geochemical features of the zircons (Table 5 and Figs. 9 and 10) support the proposed model by showing typical mantle values of Y and the sum of REE (both less than 1,000 ppm and 10,000, respectively) in the Cretaceous grains, as well as in the inherited Lower Paleozoic grains from AvQ111. The increase of U and Th in the subvolcanic rocks of the Medet deposit is related to the degree of differentiation: the higher values are typically found in the more acidic varieties (AvQ112, AvQ038 and AvQ40). The contamination with basement zircons is more characteristic for the evolved rocks and the dyke AvQ210.

The rare earth element distributions in the studied zircons from the five rock types of the Medet deposit can also be used to qualitatively estimate the oxidation state of the magma. Despite some possible analytical uncertainties, the positive Ce-anomaly (estimated by the Ce/Ce* ratio) in the mineralized rocks (AvQ111, AvQ112, AvQ038 and AvQ40) argues for zircon crystallization from a generally more oxidized magma compared to the later Q-granodiorite porphyry dyke (AvQ210). This tendency is confirmed by the Eu/Eu* ratios in the studied zircons. As previously shown by many authors (e.g. Ulrich et al. 1999; Ballard et al. 2002; Kouzmanov et al. 2006), Cu and Au will accumulate in the residual melt phase during differentiation under oxidizing conditions and finally partition into the magmatic–hydrothermal fluid phase when the magma reaches fluid saturation. In more reduced magmas, Cu will be fixed in sulfides during the magmatic crystallization and can not partition into a potentially ore-forming magmatic fluid. Thus, all other factors being equal, oxidized hydrous magmas will contain higher concentrations of Cu and Au when exsolving a late-stage fluid phase compared to their more reduced counterparts. Such a scenario is plausible for the main rock types of the Medet deposit, which contained economic concentrations of Cu and traces of Au.

With the discussion of the oxidation state we make the link from the magma characteristics to the formation of the Medet deposit. In our model of magma evolution all main rock varieties—Q-monzodiorite, Pl- and Hbl-Pl granodiorites and the aplite veins are products of a fertile magma. We defined the late dyke of Q-granodiorite porphyry as "barren", because it does not host economic mineralization. In fact, if looking only on the whole-rock characteristics or even on the Hf-zircon isotope values it would be impossible to distinguish between "fertile" and "barren" magmas. Only the oxidation state of the magma was comparatively lower in the latter one. Therefore, the specific ore-bearing features of the subduction-related magma, which is generally well known as possible source of porphyry copper deposits worldwide, may change in different regions.

One of the most important factors to form a deposit such as Medet from fertile magma is the tectonic regime. Our structural data (Fig. 3) show a change in the palaeostress field during the intrusion of various dyke generations, which are related to the pluton. The initial stage indicates an E–W extension likely associated with N–S compression followed by the late granodiorite dyke formed in an N–S extension field. As the latter is dated at 89.26±0.32 Ma, the change in paleostress orientations is, therefore, bracketed between 90.12±0.36 and 89.26±0.32 Ma. The structural data evidence a large-scale switch of external stress conditions during formation of the Medet ore deposits. Such a switch in paleostress conditions seems to be typical for major mineralized areas worldwide (e.g. Cox et al. 2001; Tosdal and Richards 2001) because it allows channelling of fluids and an increase in effective permeability.

Conclusions

1. The Upper Cretaceous ore-producing magmatism in the Medet porphyry copper deposit extended for less than 1.12 Ma and is bracketed between 90.59±0.29 Ma (the intrusion of the Q-monzodiorite porphyry) and 90.12±0.36 Ma (aplite veins) by precise ID-TIMS U–Pb-zircon dating.
2. The later Q-granodiorite porphyry dyke with an age of 89.26±0.32 Ma crosscuts the slightly older Upper Cretaceous units and only contains low-temperature ore mineralization of non-economic grade.

3. The fertile magmas in Medet assimilated Lower Paleozoic rocks with mantle-to-mantle-crustal origin (probably in a lower-crustal magma chamber), resulting in ε-Hf zircon values mainly in the range 0 to +3. The evolving magma was additionally contaminated with basement rocks in an upper crustal magma chamber.
4. Important factors controlling, the formation of the porphyry copper (Mo–Au) deposit may have been the higher oxidation state of the magma as estimated from the Ce/Ce* and the Eu/Eu* ratios in the zircons, as well as the large-scale switch of the external stress regime during the intrusion of the Medet pluton and its dykes.

Acknowledgments The authors thank the geological staff of "Assarel-Medet" AD for their kind support during fieldwork. Part of this work was supported by grant 2-77689-00 of the Swiss National Science Foundation SNF and SNF-SCOPES grants 7BUPJ062396 and 7BUPJ062276. F. Neubauer acknowledges support by grant no. 10.546 of the Austrian Science Foundation (FWF). Robert Moritz and Denis Fontignie contributed to the Sr/Nd and trace element analytical data of sample AvQ038. The English corrections of Philipp Weis and Veronika Klemm are greatly appreciated. Andreas Möller and Johann Raith (as editors) and the reviewers David Chew, and Michiel van Dongan are thanked for their constructive corrections that helped to improve the manuscript. The research is a contribution to the ESF Program "Geodynamics and Ore Deposit Evolution".

References

Angelkov K (1982) Molybdenum–copper deposit Medet. Guide to the excursion 1–3. Central Srednogorie, 13 Congress of International Mineralogical Association, Bulgarian Academy of Sciences, Sofia, 48–59 (in Russian)

Angelkov K (1984) Molybdenum–copper deposit Medet. In: Dragov P, Kolkovski B (eds) Twelve ore deposits of Bulgaria. Bulgarian Academy of Sciences, Sofia, pp 99–109 (in Russian)

Ballard JR, Palin MJ, Campbell JH (2002) Relative oxidation states of magmas inferred from Ce(IV)/Ce(III) in zircon: application to porphyry copper deposits of Northern Chile. Contrib Mineral Petrol 144:347–364

Boccalett M, Manetti P, Peccerillo A, Stanisheva-Vassileva G (1978) Late Cretaceous high-potassium volcanism in eastern Srednogorie, Bulgaria. Geol Soc Am Bull 89:439–447

Bogdanov B (1987) Copper deposits in Bulgaria. Technica, Sofia 388 p. (in Bulgarian)

Belousova E, Griffin W, O'Reylly S, Fisher N (2002) Igneous zircon: trace element composition as an indicator of source rock type. Contrib Mineral Petrol 143:602–622

Berza T, Constantinescu E, Vlad S-N (1998) Upper Cretaceous magmatic series and associated mineralisation in the Carpathian–Balkan region. Resour Geol 48:291–306

Blichert-Toft J, Albarède F (1997) The Lu–Hf isotope geochemistry of chondrites and the evolution of the mantle–crust system. Earth Planet Sci Lett 148:243–258

Bojadjiev S (1993) Comparison and petrological correlation of the South-Bulgarian granitoids. J Bulg Geol Soc 54:19–35

Carrigan C, Mukasa S, Haydoutov I, Kolcheva K (2006) Neoproterozoic magmatism and Carboniferous high-grade metamorphism in the Sredna Gora Zone, Bulgaria: An extension of the Gondwana-derived Avalonian–Cadomian belt? Precamb Res 147:404–416

Carrigan CW, Mukasa SB, Haydoutov I, Kolcheva K (2005) Age of Variscan magmatism from the Balkan sector of the orogen, central Bulgaria. Lithos 82:125–147

Cathles LM, Erendi AJH, Barrie T (1997) How long can a hydrothermal system be sustained by a single intrusive event? Econ Geol 92:766–771

Chambefort I, Moritz R (2006) Late Cretaceous structural control and Alpine overprint of the high-sulfidation Cu–Au epithermal Chelopech deposit, Srednogorie belt, Bulgaria. Miner Depos 41:259–280

Chipchakova S (2002) Wall-rock alterations in the Medet porphyry-copper deposit, Central Srednogorie. Geochem Mineral Petrol 39:67–74 (in Bulgarian with English abstract)

Chipchakova S, Lilov L (1976) About the age of the Upper Cretaceous magmatites from the western parts of Central Srednogorie and the related ore mineralizations. Compt Rend Acad Bulg Sci 29/1:101–104 (in Russian)

Ciobanu CL, Cook NG, Stein H (2002) Regional setting and Re–Os age of ores at Ocna de Fier Dognecea (Romania) in the context of the banatitic magmatic and metallogenic belt. Miner Depos 37:541–567

Cox S, Knackstedt M, Braun J (2001) Principles of structural control on permeability and fluid flow in hydrothermal systems. In: Tosdal R, Richards J (eds) Structural controls on ore genesis. Reviews in economic geology, vol. 14. Society of Economic Geologists, Littleton, CO, pp 1–24

Daieva L, Chipchakova S (1999) Geochemical peculiarities of the Upper Cretaceous magmatic rocks in the Panagyurishte volcano-intrusive region, Central Srednogorie. Geochem Mineral Petrol 37:65–76 (in Bulgarian with English abstract)

David K, Frank M, O'Nions R, Belshaw N, Arden J (2001) The Hf isotope composition of global seawater and the evolution of Hf isotopes in the deep Pacific Ocean from Fe–Mn crusts. Chem Geol 178:23–42

Dabovski C, Zagorchev I, Rouseva M, Chounev D (1972) Paleozoic granitoids in Sushtinska Sredna Gora. Ann Comm Geol Explor 16:57–92 (in Bulgarian)

DePaolo DJ (1988) Neodymium isotope geochemistry. Springer, Berlin, p 187

Dimitrova E, Belmustakova H (1982) Metamorphic facies of the crystalline schist complex of Ihtiman Sredna Gora Mountains. Geochem Mineral Petrol 16:61–67 (in Bulgarian with English abstract)

Faure G (2001) Origin of igneous rocks: the isotopic evidence. Springerp Berlin 496 pp

Georgiev S (2008) Sources and evolution of Late Cretaceous magmatism in Eastern Srednogorie, Bulgaria: constraints from petrology, isotope geochemistry and geochronology. Ph.D. thesis, Diss ETH Nr 17778, ETH Zurich, 270 pp

Günther D, von Quadt A, Wirz R, Cousin H, Dietrich V (2001) Elemental analyses using laser ablation-inductively coupled plasma-mass spectrometry (LA-ICP-MS) of geological samples fused with $Li_2B_4O_7$ and calibrated without matrix-matched standards. Mikrochim Acta 136:101–107

Halter W, Bain N, Becker K, Heinrich CA, Landtwing M, von Quadt A, Clark AH, Sasso AM, Bissig T, Tosdal RM (2004) From andesitic volcanism to the formation of a porphyry Cu–Au mineralizing magma chamber: the Farallón Negro volcanic complex, northwestern Argentina. J Volcanol Geotherm Res 136:1–30

Handler R, Neubauer F, Velichkova S, Ivanov Z (2004) $^{40}Ar/^{39}Ar$ age constraints on the timing of magmatism in the Panagyurishte region, Bulgaria. Swiss Bull Mineral Petrol 84:119–132

Harris A, Allen C, Bryan S, Campbell I, Holcombe R, Palin J (2004) ELA-ICP-MS U–Pb zircon geochronology of regional volcanism hosting the Bajo de la Alumbrera Cu–Au deposit: implications for porphyry-related mineralization. Miner Depos 39:46–97

Harris A, Dunlap W, Reiners P, Allen C, Cooke D, White N, Campbell I, Golding S (2008) Multimillion year thermal history of a porphyry copper deposit: application of U–Pb, $^{40}Ar/^{39}Ar$ and (U–Th)/He chronometers, Bajo de la Alumbrera copper–gold deposit, Argentina. Miner Depos 43:295–314

Harris N, Pearce J, Tindle A (1986) Geochemical characteristics of collision-zone magmatism. In: Coward M, Ries A (eds) Collision tectonics. Geological Society, London, special publications, vol 19. Geological Society, London, pp 67–81

Hart S, Zindler A (1989) Constraints on the nature and development of chemical heterogeneities in the mantle. In: Peltier W (ed) Mantle convection. Gordon and Breach Science, New York, pp 261–382

Heinrich CA, Neubauer F (2002) Cu–Au–Pb–Zn–Ag metallogeny of the Alpine–Balkan–Carpathian–Dinaride geodynamic province. Miner Depos 37:533–540

Hildreth W, Moorbath S (1988) Crustal contributions to arc magmatism in the Andes of central Chile. Contrib Mineral Petrol 98:455–489

Hoskin P, Ireland T (2000) Rare earth chemistry of zircon and its use as a provenance indicator. Geology 28:627–630

Hoskin P, Schaltegger U (2003) The composition of zircon in igneous and metamorphic petrogenesis. In: Hanchar J, Hoskin P (eds) Zircon. Reviews in mineralogy and geochemistry, vol 53. Mineralogical Society of America, Washington, pp 27–62

Ignatovski P (1979) Structure of the copper-porphyry deposit Assarel. J Bulg Geol Soc 9:263–277 (in Bulgarian)

Janković S (1977) The copper deposits and geotectonic setting of the Tethyan Eurasian metallogenic belt. Miner Depos 12:37–47

Kamenov B, Yanev Y, Nedialkov R, Moritz R, Peytcheva I, von Quadt A, Stoykov S, Zartova A (2007) Petrology of Late-Cretaceous island-arc ore-magmatic centers from Central Srednogorie, Bulgaria: magma evolution and paths. Geochem Mineral Petrol 45:39–77

Kouzmanov K, von Quadt A, Peytcheva I, Heinrich CA, Pettke T, Rosu E (2006) Geochemical and time constraints on porphyry ore formation in the Barza magmatic complex, Apuseni Mountains, Romania. In: Cook NJ, Ozgenc I, Oyman T (eds) Au–Ag–Te–Se deposits. Proceedings of the 2006 Field Workshop, IGCP Project 486, Izmir, Turkey, 24–29 September, 96–102

Lilov P, Chipchkova S (1999) K–Ar dating of the Upper Cretaceous magmatic rocks and hydrothermal metasomatic rocks from the Central Srednogorie. Geochem Mineral Petrol 36:77–91 (in Bulgarian with English abstract)

Lips A (2002) Correlating magmatic–hydrothermal ore deposit formation over time with geodynamic processes in SE Europe. In: Blundell D, Neubauer F, von Quadt A (eds) The timing and location of major ore deposits in an evolving orogen. Geological Society, London, special publications, vol 204. Geological Society, London, pp 69–79

Lips A, Herrington R, Stein G, Kozelj D, Popov K (2004) Refined timing of porphyry copper formation in the Serbian and Bulgarian portions of the Cretaceous Carpatho–Balkan belt. Econ Geol 99:601–609

Ludwig KR (1988) PBDAT for MS-DOS; a computer program for IBM-PC compatibles for processing raw Pb–U–Th isotope data, version 1.00a. US Geological Survey, Reston, VA 37 pp

Ludwig KR (2003) Isoplot/Ex—a geochronological toolkit for microsoft excel. Berkeley Geochronol Centre Spec Publ 4:1–71

Marsh TM, Einaudi MT, McWilliams M (1997) $^{40}Ar/^{39}Ar$ geochronology of Cu–Au and Au–Ag mineralization in the Potreillos district, Chile. Econ Geol 92:784–806

Mattinson J (2005) Zircon U–Pb chemical abrasion ("CA-TIMS") method: combined annealing and multi-step partial dissolution analysis for improved precision and accuracy of zircon ages. Chem Geol 220:47–66

Milev V, Stanev V, Ivanov V (1996) Statistical manual of the ore production in Bulgaria during 1878–1995. Zemia 99, Sofia, p 196 (in Bulgarian)

Murray A, Guillong M, Meier D, Hanley J, Heinrich CA, Yardley B (2007) LA-ICP-MS analysis of inclusions: improved data reduction capabilities. ECROFI-XIX 1, p. 186

Neubauer F (2002) Contrasting Late Cretaceous with Neogene ore provinces in the Alpine–Balkan–Carpathian–Dinaride collision belt. In: Blundell D, Neubauer F, von Quadt A (eds) The timing and location of major ore deposits in an evolving orogen. Geological Society, London, special publications, vol . vol. 204. Geological Society, London, pp 81–102

Neubauer F, Heinrich CA, ABCD-GEODE working group (2003) Late Cretaceous and Tertiary geodynamics and ore deposit evolution of the Alpine–Balkan–Carpathian–Dinaride orogen. In: Eliopoulos et al (ed) Mineral exploration and sustainable development. Millpress, Rotterdam, pp 1133–1136

Ortner H, Reiter F, Acs P (2002) Easy handling of tectonic data: the programs Tectonics VP for Mac and Tectonics FP for Windows. Comp Geosci 28:1193–1200

Parrish R, Noble S (2003) Zircon U–Th–Pb geochronology by isotope dilution—thermal ionization mass spectrometry (ID-TIMS). In: Hanchar J, Hoskin P (eds) Zircon. Reviews in Mineralogy and Geochemistry, vol 53. Mineralogical Society of America, Washington, pp 183–241

Pearce J, Harris N, Tindle A (1984) Trace element discrimination diagrams for tectonic interpretation of granitic rocks. J Petrol 25:956–983

Pearce N, Perkins W, Westgate J, Gorton M, Jackson S, Neal C, Chenery S (1997) A compilation of new and published major and trace element data for NIST SRM 610 and NIST SRM 612 glass reference materials. Geostand Newslett 21:115–141

Peytcheva I, von Quadt A (2004) The Paleozoic protoliths of Central Srednogorie, Bulgaria: records in zircons from basement rocks and Cretaceous magmatites. Proceedings of the 5th Intern Symp Eastern Mediterran Geol, 14–20.04.2004, Thessaloniki, Greece, 1:392–395

Peytcheva I, von Quadt A, Georgiev N, Ivanov Z, Heinrich CA, Frank M (2008) Combining trace-element compositions, U–Pb geochronology and Hf isotopes in zircons to unravel complex calcalkaline magma chambers as inferred by mixed gabbros and granodiorites in the Upper Cretaceous Srednogorie zone (Bulgaria). Lithos 104:405–427

Popov P, Bayraktarov I (1978) Structural features of the copper-molybdenum deposit Medet. Ann Univ Min Geol 23/2:77–98

Popov P, Strashimirov S, Arnaudova R, Kanazirski M, Popov K (1996) Geology and genetic model of the porphyry copper deposits from the Assarel-Medet ore field. In: Popov P (ed) Plate tectonic aspects of the Alpine metallogeny in the Carpatho-Balkan region. UNESCO-IGCP Project 356, Proceedings Ann Meet, Sofia, 1:175–196

Popov P, Popov K (2000) General geologic and metallogenic features of the Panagyurishte ore region. In: Strashimirov S, Popov P (eds) Geology and metallogeny of the Panagyurishte ore region. Guide to excursions A and C, ABCD-GEODE 2000 workshop, Borovets, pp. 19–25

Popov P, Berza T, Grubic A (2000a) Upper Cretaceous Apuseni–Banat–Timok–Srednogorie (ABTS) magmatic and metallogenic belt in the Carpathian–Balkan orogen. Abastr Vol ABCD-GEODE workshop, Borovets, p. 69

Popov P, Strashimirov S, Kanazirski M (2000b) Assarel-Medet ore field. In: Strashimirov S, Popov P (eds) Geology and metallogeny of the Panagyurishte ore region. Guide to excursions A and C, ABCD-GEODE 2000 workshop, Borovets, pp. 1–7

Sandulescu M (1984) Geotectonica Rumaniei. Editura Technica, Bucuresti, p 336

Schmid S, Bernoulli D, Fügenschuh B, Matenco L, Schefer S, Schuster R, Tischler M, Ustaszewski K (2008) The Alpine–Carpathian–Dinaridic orogen system: correlation and evolution of tectonic units. Swiss J Geosci 101:139–183

Segal I, Halicz L, Platzner IT (2003) Accurate isotope ratio measurements of ytterbium by multiple collection inductively coupled plasma mass spectrometry applying erbium and hafnium in an improved double external normalization procedure. J Anal Spectrom 18:1217–1223

Sláma J, Košler J, Condon D, Crowley JL, Gerdes A, Hanchar JM, Horstwood M, Morris G, Nasdala L, Norberg N, Schaltegger U, Schoene B, Tubrett M, Whitehouse M (2008) Plešovice zircon—a new natural reference material for U–Pb and Hf isotopic microanalysis. Chem Geol 249:1–35

Stacey JS, Kramers JD (1975) Approximation of terrestrial lead isotope evolution by a two-stage model. Earth Planet Sci Lett 26:207–221

Steiger R, Jäger E (1977) Subcommission on geochronology: convention on the use of decay constants in geo- and cosmochronology. Earth Planet Sci Lett 36:359–362

Stoykov S, Peytcheva I, von Quadt A, Moritz R, Fontignié D (2004) Timing and magma evolution of the Chelopech volcanic complex (Bulgaria). Swiss Bull Miner Petrol 84:101–117

Strashimirov S (1982) Mineral associations, conditions and development of ore-forming processes in the porphyry-copper deposit Medet. Ph. D. thesis summary, Sofia, 34 pp (in Bulgarian)

Strashimirov S, Kovachev V (1992) Temperature of formation in copper deposits from the Srednogorie zone—data from fluid inclusion studies in minerals. Rev Bulg Geol Soc 53/2:1–12 (in Bulgarian)

Strashimirov S, Popov P (2000) Geology and metallogeny of the Panagyurishte ore region (Srednogorie Zone, Bulgaria). Guide to excursions A and C, ABCD-GEODE workshop, Borovets, Bulgaria, p. 50

Strashimirov S, Petrunov R, Kanazirski M (2002) Porphyry-copper mineralization in the central Srednogorie zone, Bulgaria. Miner Depos 37:587–598

Sun S, McDonough W (1989) Chemical and isotopic systematics of oceanic basalts: implications for mantle compositions and processes. In: Saunders A, Norry M (eds) Magmatism in ocean basins. Geological Society, London, special publications, vol 42. Geological Society, London, pp 313–345

Tarkian M, Stribrny B (1999) Platinum-group elements in porphyry copper deposits: a reconnaissance study. Mineral Petrol 65:161–183

Tosdal R, Richards J (2001) Magmatic and structural controls on the development of porphyry Cu ± Mo ± Au deposits. In: Tosdal R, Richards J (eds) Structural controls on ore genesis. Reviews in economic geology, vol. 14. Society of Economic Geologists, Littleton, CO, pp 157–181

Tsvetkov K, Yossifov D, Obretenov N (1978) Characteristics of the main ore-controlling structure in Central Srednogorie. J Bulg Geol Soc 39:41–50

Ulrich T, Günther D, Heinrich CA (1999) Gold concentrations of magmatic brines and the metal budget of porphyry copper deposits. Nature 399:676–679

Ushev A, Chipchakova S, Angelkov K (1962) The Medet pluton and the connected copper-porphyry deposit, Panagyurishte district. In: Contribution to the Geology of Bulgaria 1:69–148 (in Bulgarian)

Vassileff L, Stanisheva-Vassileva G (1981) Metallogeny of the Eurasian copper belt: Sector Bulgaria. Geol Balc 11:73–87

Vavra G (1990) On the kinematics of zircon growth and its petrogenetic significance: a cathodeluminescence study. Contrib Mineral Petrol 106:90–99

von Quadt A, Peytcheva I, Kamenov B, Fanger L, Heinrich CA, Frank M (2002) The Elatsite porphyry copper deposit in the Panagyurishte ore district, Srednogorie zone, Bulgaria: U–Pb zircon geochronology and isotope-geochemical investigations of magmatism and ore genesis. In: Blundell DJ, Neubauer F, von Quadt A (eds) The timing and location of major ore deposits in an evolving orogen. Geological Society, London, special publications, vol 204. Geological Society, London, pp 119–135

von Quadt A, Moritz R, Peytcheva I, Heinrich CA (2005) Geochronology and geodynamics of Late Cretaceous magmatism and Cu–Au mineralization in the Panagyurishte region of the Apuseni–Banat–Timok–Srednogorie belt (Bulgaria). Ore Geol Rev 27:95–126

Wortel M, Spakman W (2000) Subduction and slab detachment in the Mediterranean–Carpathian region. Science 290:1017–1910

Zimmerman A, Stein H, Hannah J, Koželj D, Bogdanov K, Berza T (2008) Tectonic configuration of the Apuseni–Banat–Timok–Srednogorie belt, Balkans–South Carpathians, constrained by high precision Re–Os molybdenite ages. Miner Depos 43:1–21

Zindler A, Hart S (1986) Chemical geodynamics. Ann Rev Earth Planet Sci 14:493–571